General Disclaimer

One or more of the Following Statements may affect this Document

- This document has been reproduced from the best copy furnished by the organizational source. It is being released in the interest of making available as much information as possible.

- This document may contain data, which exceeds the sheet parameters. It was furnished in this condition by the organizational source and is the best copy available.

- This document may contain tone-on-tone or color graphs, charts and/or pictures, which have been reproduced in black and white.

- This document is paginated as submitted by the original source.

- Portions of this document are not fully legible due to the historical nature of some of the material. However, it is the best reproduction available from the original submission.

OLD DOMINION UNIVERSITY RESEARCH FOUNDATION

DEPARTMENT OF PHYSICS AND GEOPHYSICAL SCIENCES
SCHOOL OF SCIENCES
OLD DOMINION UNIVERSITY
NORFOLK, VIRGINIA

Technical Report PGS-TR-PH-75-12

A THEORETICAL/EXPERIMENTAL PROGRAM TO DEVELOP ACTIVE OPTICAL POLLUTION SENSORS: QUANTITATIVE REMOTE RAMAN LIDAR MEASUREMENTS OF POLLUTANTS FROM STATIONARY SOURCES

By

S.K. Poultney

M.L. Brumfield

and

J.S. Siviter

Annual Report

Prepared for the
National Aeronautics and Space Administration
Langley Research Center
Hampton, Virginia

Under
Grant NSG 1060
June 1, 1974 - May 31, 1975

October 1975

DEPARTMENT OF PHYSICS AND GEOPHYSICAL SCIENCES
SCHOOL OF SCIENCES
OLD DOMINION UNIVERSITY
NORFOLK, VIRGINIA

Technical Report PGS-TR-PH-75-12

A THEORETICAL/EXPERIMENTAL PROGRAM TO DEVELOP ACTIVE OPTICAL POLLUTION SENSORS: QUANTITATIVE REMOTE RAMAN LIDAR MEASUREMENTS OF POLLUTANTS FROM STATIONARY SOURCES

By

S.K. Poultney

M.L. Brumfield

and

J.S. Siviter

Annual Report

Prepared for the
National Aeronautics and Space Administration
Langley Research Center
Hampton, Virginia 23665

Under
Grant NSG 1060
June 1, 1974 - May 31, 1975
Dr. E. Remsberg, Technical Monitor
Environmental and Space
Sciences Division

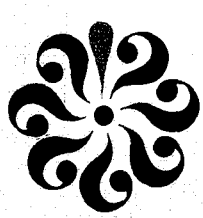

Submitted by the
Old Dominion University Research Foundation
Norfolk, Virginia 23508

October 1975

SUMMARY

Typical pollutant gas concentrations at the stack exits of stationary sources can be estimated to be about 500 ppm under the present emission standards. Raman lidar has a number of advantages which makes it a valuable tool for remote measurements of these stack emissions. Tests of the Langley Research Center Raman lidar at a calibration tank indicate that night measurements of SO_2 concentrations and stack opacity are possible. Accuracies of 10 percent are shown to be achievable from a distance of 300 m within 30 min integration times for 500 ppm SO_2 at the stack exits. All possible interferences were examined quantitatively (except for the fluorescence of aerosols in actual stack emissions) and found to have negligible effect on the measurements. An early test at an instrumented stack is strongly recommended.

CONTENTS

CONTENTS - concluded

LIST OF TABLES

LIST OF FIGURES

LIST OF FIGURES - concluded

REMOTE MEASUREMENTS OF POLLUTANTS FROM STATIONARY SOURCES USING RAMAN LIDAR

By

S.K. Poultney[1], M.L. Brumfield[2], and J.S. Siviter[2]

1. INTRODUCTION

Two types of stationary sources contribute to regional pollution throughout the country if adequate controls are not used. These are fossil fuel power plants and municipal incinerators. Smelters, pulp mills, and petroleum refineries can also contribute in particular locations. The emissions which lead to pollution consist of both gases and particulates. The primary gases are SO_2, NO, and HCl. Subsequent dispersion and reaction of these components and others can lead to sulfurous smogs and contribute to photochemical smogs with their attendant effects on man and property. Regional air quality standards have led to emission standards for existing stationary sources. Estimates of the emissions from the various sources can be made by knowing general information about the activity at the source, the type of fuel, and the control devices in use. Many of the operators of stationary sources will monitor the emissions to stay within emission standards and to check the efficacy of their control devices. However, the general community may want to verify the compliance of each stationary source with the emission standards by independent measures from a remote location.

---

[1] Department of Physics and Geophysical Sciences, Old Dominion University, Norfolk, Virginia 23508.

[2] NASA Langley Research Center, Hampton, Virginia 23665.

Raman lidar has a number of advantages which makes it a valuable tool for remote measurements of these stack emissions. The typical pollutant gas concentrations at the stack exit (e.g., 500 ppm in the absence of controls) can be monitored by means of Raman-scattered light from the illuminating laser beam in spite of the rather low cross sections for the scattering process. The measurements are possible at the typical stack height of several hundred meters from a remote location and are specific to the gas in question. The illuminating laser need not be tuned nor narrowed as in other schemes. Supplementary measurements of stack plume cross section and stack exit velocity must be made in order to derive the concentration and mass emission rate. The plume diameter can be obtained using a separate channel of the Raman lidar. Lidar calibration to obtain absolute values can be achieved in several ways. One can operate two or more simultaneous return channels with one being ambient nitrogen outside the plume. The relative sensitivity of the channels can be periodically checked by viewing a standard lamp. Alternately, one could operate a single channel viewing the pollutant in the plume and then oxygen outside the plume. This latter method is most convenient for SO_2 measurements.

Two types of interference must be guarded against: leakage of the wrong wavelength return or acceptance of aerosol broad-band fluorescence into the spectral bandwidth of a receiver channel. The leakage can be controlled by proper design of the spectral selection elements in the lidar receiver. Fluorescence may not be a problem for stacks with particulate control devices or for longer wavelength lasers. It can be identified by looking for scattered light at wavelengths not characteristic of Raman scatter and for signals decaying with a characteristic fluorescence time constant. Both of these possible interferences as well as the actual performance of the Raman stack monitor lidar can be checked at a calibration tank facility before measurements at a stack. This report describes a particular Raman lidar and its performance at the calibration tank facility. This Raman lidar is capable of

night measurements of SO_2 and HCl under the conditions mentioned above to an accuracy of 10 percent within 30 min from a distance of 300 m. Its performance for SO_2 has been independently measured in a calibration facility for the first time. This report does not address directly the issue of what laser should be used for the optimum Raman lidar for either performance or eye safety. The particular lidar described here can be used for day measurements only if a different data acquisition scheme were to be used.

The measurement of stack particulates most accessible to a Raman lidar is that of stack opacity. The Raman return from nitrogen (or oxygen) in the range cells before the stack and the range cells after the stack can yield the extinction or opacity of the stack plume. The use of a Raman lidar for this measurement may eliminate certain problems associated with other lidar means. Concentration and mass emission rates are more difficult to obtain by lidar means. In addition to the supplementary measurements needed for pollutants, one must know or measure the optical properties of the particles involved. Lidar can easily provide only two parameters related to particle concentration and properties; extinction and backscatter. The measurement of particulate mass emission rate has been addressed by several authors, but will not be discussed here.

2. STATIONARY SOURCE EMISSIONS AND EMISSION STANDARDS

2A. Estimates of Emissions from Power Plants and Municipal Incinerators

Emissions from the stationary source fossil fuel power plants and municipal incinerators will be discussed in this section. The amount of these emissions can be estimated by knowing general information about the activity, fuel, and control devices of the particular source (ref. 1). Uncertainty about any of these components or their use requires remote measurements to check independently compliance with emission standards. Fossil fuel power plants use gas, oil, coal, or a combination of these three fuels. A municipal

incinerator might also be used as a power plant. Its fuel would be rubbish. Each fuel has an emission factor which indicates how much pollutant is emitted for a given amount of fuel burned. This factor in the case of SO_2 depends on the sulfur content of the particular lot of fuel. Table 1 lists the emission factors and caloric values for the several fuels except gas which is very clean. The percent sulfur, fly ash, and chlorine in the respective entries is represented by the letter s. For example, 1 percent sulfur coal would yield 2.7 kg of SO_2 for the conditions stated in table 1. The amount of NO_x emitted depends on the flame temperature at which the fuel burns. Table 1 also lists the actual amount of pollutant emitted per 4.186 GJ heat input (also written GJh). The emitted amount in grams will be seen to be closely related to the present emission standards. The above heat input each second represents a large modern 1.7 GWe power plant, assuming an efficiency of 40 percent.

One can estimate the pollutant mass emission rates and concentrations near the top of the stack if one knows the rate at which the power plant in question uses fuel. Table 2 lists the rates and concentrations for the modern 1.7 GWe power plant. Calculation of the mass emission rates is straightforward. Calculation of the concentration requires additional assumptions. The concentration in the plume at the stack exit is given by

$$C = Q_V/vA \tag{1}$$

where C is the concentration in ppm, Q_V the volume emission rate in m^3/sec, v the exit velocity in m/sec, and A the plume area in m^2 right above the stack exit. It is assumed here that v equals 100 km/hr and A corresponds to a stack diameter of 10 m. The volume emission rates for gases are obtained from the mass emission rates using

$$Q_V = 22.4 \times 10^{-3} \ (Q_M/M_P) \ (T/273) \tag{2}$$

Table 1. Stationary Source Emissions. Values taken or calculated from Williamson (ref. 1). The sulfur, chlorine, and fly ash content of actual fuel used is specified by s in percent. The amount of pollutant emitted is calculated for a heat input of 4.186 GJ, which is typical of modern large power plants with 1.7 GWe capacities.

	Petroleum	Coal	Rubbish
Emission Factors			
SO_2	19s g/liter	19s kg/tonne	1 kg/tonne
NO_2	12 g/liter	10 kg/tonne	1 kg/tonne
Particulates	1.2 g/liter	8s kg/tonne	15 kg/tonne
HCl	---	10s kg/tonne	10s kg/tonne
Caloric Value	4.2×10^7 J/liter	30×10^9 J/tonne	11×10^9 J/tonne
Amount of Pollutant Emitted			
SO_2	2.0s kg	2.7s kg	0.38 kg
NO_2	0.13 kg	1.4 kg	0.38 kg
Particulates	0.12 kg	8.2s kg	5.7 kg
HCl	---	1.3s kg	3.8s kg

Table 2. Fossil Fuel Power Plant Mass Emission Rates and Plume Pollutant Concentrations at Stack Exit. Values calculated from Williamson (ref. 1). Plant is 1.7 GWe capacity operating at 40 percent efficiency with a 10 m diameter plume at exit and a 100 km/hr exit velocity. Stacks are assumed to have a 99.7 percent particle precipitator.

Fuel	SO_2	NO_x	Particulates	HCl
Petroleum	400 ppm	38 ppm	--	--
1% S	(2.0 kg/sec)	(0.13 kg/sec)	(0.36 g/sec)	--
Coal				
1% S	540 ppm	380 ppm	--	230 ppm
1% fly ash	(2.7 kg/sec)	(1.4 kg/sec)	(49 g/sec)	(0.68 kg/sec)
0.5% Cl				
Rubbish				
3% plastic	75 ppm	110 ppm	--	680 ppm
0.5% Cl	(0.38 kg/sec)	(0.38 kg/sec)	(17 g/sec)	(1.9 kg/sec)

where Q indicates the respective rates, the units of Q_M are kg/sec, M_p is the molecular weight of the pollutant in kg, and T is the exit plume temperature in °K. It is assumed here that the plume temperature is 413° K. The fuel is assumed to be 1 percent sulfur and, in the case of coal, 1 percent fly ash. Similar calculations are done for HCl from plants burning 0.5 percent Cl coal and rubbish with 3 percent plastic component. Note that the HCl emission from a municipal incinerator may be an order of magnitude higher if plastics with high polyvinyl chloride components are burned.

The following observations can be made based on table 2. The SO_2 concentrations at the top of large, modern power plants (e.g., 1.7 GWe) without controls are about 500 ppm for 1 percent sulfur fuel which is just in the range of remote Raman lidar. The difficulty of disposing of acid liquid wastes means that these SO_2 concentrations will not be reduced by controls except if the sulfur is removed from the fuel before use or if it can be commercially recovered from the wastes right at the plant. Relaxation of present emission standards for coal plants due to the energy crisis could increase SO_2 concentrations dramatically since coal can have sulfur contents as high as 7 percent. Such relaxation would, however, require either modification of stack design or use of control devices because the increased emissions may impinge on the ambient air quality standards as discussed in section 2C. The NO_x concentration is relatively high for a coal stack, but it turns out that the Raman cross section for NO (the form of NO_x at the stack exit) is an order of magnitude below that of SO_2. Raman lidar measurements of NO are therefore not promising. Table 2 indicates that HCl up to the 250 ppm level might be present in coal stack emissions for 0.5 percent Cl coal. The higher HCl concentrations (e.g., 700 ppm) in the plume from a municipal incinerator power plant of the dimensions stated above should be even more accessible to the Raman lidar. Particulate mass emission rates are also given under the assumption of 99.7 percent efficient precipitators.

The above estimates for stack plume concentrations of pollutants have been made for large modern power plants operating at full capacity. One might ask what concentrations are expected for the older 200 MWe power plants and what concentrations are expected when either size plant reduces its power output. By equation (1), the expected concentration depends on the mass emission rate, the exit velocity, and the stack area. The mass emission rate has an obvious relation to power plant capacity and output. Changes in operating power levels at a plant will change the concentrations of pollutants in the plume directly with the change in emission rate if the exit velocity is kept the same. At many plants, the exit velocity is decreased as the output level is decreased so that the pollutant concentration in the plume may stay the same. A measurement of stack exit velocity is essential if Raman lidar concentration measurements are to be related to the required mass emission rates. The 200 MWe power plants have one-tenth the mass emission rates of the large plants by definition, but their stack sizes are scaled down from the sizes of the stacks at the large plants for reasons discussed in section 2C. Typical stack diameters of the small plants are one-third those of the large plants. Equation (1) thus indicates that the pollutant concentrations are the same for large and small plants which use the same fuels. A measurement of stack plume cross section is essential to obtain the required mass emission rates from the Raman lidar concentration measurements (in addition to interpreting the lidar measurements in the first place).

2B. Emission Standards

The Federal standard of performance for fossil-fuel-fired steam generators with respect to SO_2 emission is quoted in grams of SO_2 in the emitted gases per million calorie heat input (Mcalh) (ref. 2). For liquid fossil fuel, the number is 1.4 g/Mcalh, and for solid fossil fuel, the number is 2.2 g/Mcalh. Table 1 lists the pollutant amount emitted per 1 Gcal heat input or 4.2 GJh for various fuels. To compare these estimates with the

Federal emission standards, one merely divides the amounts in table 1 by 10^3. For example, table 1 indicates that 1 percent sulfur coal emits slightly more SO_2 than allowed by the emission standard. The Federal emission standards are apparently a restriction on the sulfur content of the fuel used. The standards also do not limit the absolute amount of pollutants which a plant may emit since a plant with a larger power capacity requires a larger heat input per second. The emission standards are, of course, derived from ambient air quality considerations and do not contain the final word on stack emissions. They are a guide to the achievement of ambient air quality standards and as such are contested for various reasons by stationary source operators. It will be useful to briefly consider the issues involved to see what role Raman lidar may play in resolving the emission standards controversy.

2C. Dispersal of Stationary Source Emissions and Ambient Air Quality Standards

The ambient air quality standards of 1971 (ref. 1) are summarized in table 3 for selected pollutants. Little controversy surrounds these standards. Note that the standards are concentrations in ppm and are much lower than the stack concentrations (e.g., 0.1 ppm for SO_2). Plume dispersion processes are thus very important. Conventional plume dispersion theory predicts that the maximum ground-level pollution concentration depends directly on the pollutant emission rate (not stack concentration) and inversely on the square of the stack height (ref. 1). The increase in mass emission rate allowed the larger capacity power plants can thus be offset by proper stack design. For example, the 200 MWe plants have stacks about 100 m high, whereas the new 1.7 GWe plants have stacks about 300 m high. The maximum ground level pollutant concentration of each is probably about the same. The actual value of the ground-level concentration may vary widely. The dispersal process depends on the geographical location of the plant, the meteorological parameters of the

Table 3. Selected Air Quality Standards (Federal) 1971. From Williamson (ref. 1).

Pollutant	Averaging Time	Primary Standard	Objectives of Standards
SO_2	Annual Average	0.03 ppm	To prevent possible increase in chronic respiratory disease and damage to vegetation.
	24-hour	0.14 ppm	
NO_2	Annual Average	0.05 ppm	To prevent possible risk to public health and atmospheric discoloration.
Suspended Particulate Matter	Annual Geometric Mean	75 microgram/m^3	To improve visibility and prevent acute illness when present with about 0.05 ppm SO_2.
	24-hour	260 microgram/m^3	

atmosphere (including turbulence), the design of the plant and the stack, and chemical reactions (in the presence of particulates) that may be taking place. Even in the best of conditions, one does not expect predictions accurate to better than a factor of two over a certain averaging period. Higher concentrations over shorter times at the ground could be dangerous and could occur. Williamson (ref. 1) concludes his tutorial review of plume dispersion as follows: "A useful quantitative theory permitting the exact calculation of the downwind pollution from a point source, which incorporates measurable features of atmospheric turbulence in the intervening distance, has not yet been achieved."

Federal emission standards and designs for new power plants were undoubtedly determined by application of the present dispersion theory and by extrapolation from empirical measurements in the vicinity of existing plants. Either means raises questions which lead to the present controversy about emissions standards. First, how much credence can one place in emission standards derived from ambient air quality standards via an imperfect theory? Part of the problem in constructing a better theory is that the rapid temporal variations of the ambient concentration of pollutants cannot even be precisely measured. Neither can the meteorological parameters be measured over the time scale and over the affected area. In view of these measurement difficulties, it is natural to ask whether or not Raman lidar could obtain the necessary accuracy, range, and time resolution. For 1 ppm SO_2, the use of a Raman lidar such as the one described below would require a decrease in range to about 10 m, thereby making the lidar no longer remote. The same conclusion is true for the several meteorological parameters accessible to Raman lidar.

The empirical means for determining the emission standard immediately raises the question of why a standard other than the ambient air quality standard. Each point source would maintain a monitoring network and would operate so as to never broach the ambient standard. On good days, the source would burn high sulfur

fuel, and at bad times it would switch to low sulfur fuels (ref. 3). The problem with this approach is that pollution is usually caused by a group of point sources. The present emission standard at least means that each individual in this group maintain its proportionate share of pollution. In fact, a variable emission standard based on atmospheric conditions might not be a bad compromise. In any case, one might like to have an instrument that can check for compliance the operation of each individual point source. The Raman lidar is such an instrument.

A third possible use of Raman lidar for stack plume monitoring might come in the chemical reaction aspect of the dispersion process. For example, the SO_2 concentration might be monitored in the presence of varying amounts of particulates or other material. The lidar might, at the same time, monitor the particulate matter present.

3. RAMAN LIDAR

Raman lidar is not a new idea. Its use was first suggested by Cooney (ref. 4) in 1965 and implemented for the detection of atmospheric nitrogen by Leonard (ref. 5) in 1967. Its application to the measurement of pollutants was first proposed by Inaba and Kobayasi (ref. 6) and then realized by them (ref. 7) in 1970 for the cases of SO_2 and CO_2 in a nearby oil smoke plume. A brief summary of the use of Raman lidar for stack emission measurements is given below. First, however, the Raman scattering phenomenon will be described. Then follow a description of the LaRC Raman lidar used in the present tests and predictions of its performance for various gases. After the lidar summary, the issues of possible interferences and absolute calibration are outlined.

3A. The Raman Scattering Phenomenon

Raman scattering may be regarded as an inelastic collision between a photon of energy $h\nu_o$ and a molecule. The molecule is left in an excited state characteristic of its structure and

a photon with energy $h\nu_R = h\nu_o - \Delta E$ is emitted. The energy loss ΔE of the photon corresponds to a unique rotational or a vibration-rotation energy change in the state of the molecule. The process is sketched in figure 1 for vibrational Raman scattering. In the wavelength domain, this shift is to the long wavelength side of the exciting laser wavelength as indicated in figure 2. This paper concerns itself with the large shifts of the vibration-rotation excitation. Figure 3 indicates specific shifts for the constituents of an oil smoke plume for excitation by a ruby laser. Table 4 lists these shifts, the scattered wavelengths for ruby excitation, and more accurate scattering cross sections for a number of gases of possible interest. The cross sections have been stated relative to that of nitrogen and the appropriate corrections have been made for the wavelength dependence of Raman scattering using equation (3) and the actual excitation wavelength of measurement.

$$\sigma \sim \nu_R^4 \sim 1/\lambda_R^4 \tag{3}$$

These cross sections are quite small. For comparison, the Rayleigh scattering cross section is 1.98×10^{-28} cm^2/sr (ref. 11). The Raman cross sections are the prime determinate of the design and performance of a Raman lidar.

3B. Raman Lidar Design

The design of Raman lidars is not particularly straightforward due in part to the weak scattering cross sections and in part to many possible sources of interference. Kildal and Byer (ref. 12) and the work of the Japanese group (refs. 13, 14) give a good insight into most of the intricacies of the design although each omits certain possible interferences. A Raman lidar consists of a laser to illuminate the target gas, a telescope receiver to collect and separate the scattered light, and a data acquisition system (DAQ) to record the data. Figure 4 shows the first two components schematically and figure 5 shows the DAQ. The choice

Table 4. Raman Scatter Properties of Selected Gases. Q branch cross sections are given relative to nitrogen for 6943 Å excitation. The appropriate wavelength scaling was done from the wavelengths of actual measurement.

Gas	Raman Shift (cm^{-1})	λ_{RS} (6943) (Å)	σ_{rel} (6943)	Reference
$N_2(\nu_1)$	2331	8284	1.0	8
O_2	1556	7784	1.4	8
SO_2	1151	7546	6.6	8
NO	1876	7982	0.51	8
$CO_2(2\nu_2)$	1286	7624	1.10	8
$CO_2(\nu_1)$	1388	7683	1.59	8
CO	2143	8158	1.02	8
H_2S	2611	8480	6.4	9
$CH_4(\nu_1)$	2914	8703	7.5	9
HCl	2886	8683	2.6	10

Note: Absolute N_2 differential scattering cross section is:

$4.4\ (\pm\ 1.7) \times 10^{-31}$ cm^2/sr for 5145 Å excitation (9)

1.1×10^{-31} cm^2/sr for 6943 Å excitation.

of components is dictated to a large extent by the lidar equation (4) which predicts the signal return from a target gas based on lidar system parameters and on the concentration and cross-section of the gas. Elimination of interferences is addressed in section 5E.

The lidar equation is here expressed in terms appropriate for photon counting of the return signal. It is divided into four dimensionless factors.

$$N_{OR,i} = \left(\frac{\lambda_R}{\lambda_o}\right) \left[\frac{E_o}{hc/\lambda_o}\right] \left\{ n_2 \sigma_2(\pi) \, L_i \int_o^{R_i} \left[\exp\left(-\beta_{A_o}(tot) - \beta_{AR}(tot) \right) R \right] \cdot \pi_x \, e^{-n_x \sigma_x R} \, dR \right\} \left[\frac{AK}{4\pi R_i^2}\right] \tag{4}$$

First, there is a scale factor which adjusts the conventional lidar equation (usually expressed in terms of instantaneous power) so that the scattered signal can be expressed in counts per range time bin and the exciting pulse in photons. The second factor is the number of photons in the exciting light pulse of E_o joules leaving the laser. The third factor contains the backscatter cross section, $\sigma_2(\pi)$, the gas concentration, n_2, the length of the viewed interval, L, and any extinction along the path due to aerosol, $\beta_A(tot)$, or absorbing gas $n_x\sigma_x$. This factor assumes that the viewed interval is much longer than the exciting pulse length. Corrections are necessary if the range interval is shorter, depending on whether the gas is localized in a plume or continuously distributed. The last factor contains the total efficiency of a receiver channel, K, including the photosurface quantum efficiency and it contains the lidar geometry with A the area of the receiver and R the range to the viewed interval.

The lidar parameters used or assumed in the present design are listed in table 5. The total channel efficiency is given

Table 5. LaRC Raman Lidar Design Parameters.

Range	300 m
Range interval	6 m or 40 nsec
SO_2 concentration	1000 ppm
Laser wavelength	6943 Å
Laser energy	1.5 J or 6 x 10^{18} photons (nominal)
Laser beam divergence	1 mrad
Laser firing rate	30 ppmin
Receiver diameter	8 inches (or 0.03 m^2 in area)
Receiver field of view	3 mrad
Detection method	Photon counting
SO_2 Raman channel total efficiency, K	0.025 cts/scattered photon
Atmospheric transmission (two way)	0.8

only for the most sensitive channel viewing SO_2. The design is the result of a number of separate contributions which, however, had the same basic aims. The smallest telescope possible was chosen for compactness. This choice both required and allowed photon counting techniques to be used. Use of photon counting detection also allowed convenient use of digital elements in the DAQ (ref. 15) and narrow range bins (e.g., down to 20 nsec) (ref. 15), but limited lidar operation to night-time as will be discussed later. The DAQ configuration as shown in figure 5 includes the Tomlinson Research sixteen-bin photon counting unit (ref. 15) and an auxiliary single time bin second channel which was used for a time. The spectral selection elements were chosen to be interference filters as shown in figure 4 for compactness, ease of operation, and higher throughput than many high-rejection-ratio monochromators. The selection of a ruby laser gave the option of operation at 6943 Å or at 3472 Å at reduced energy per pulse. The choice here was 6943 Å due to the simplicity of operation, the higher pulse energies available, and the hopes of avoiding various interference problems.

The original version of the LaRC Raman lidar was described by Melfi et al. (ref. 16) and is basically the same as herein described except for certain changes and improvements. Northam and Brumfield (ref. 17) later reassembled the lidar at LaRC using a more compact 8-inch telescope because of the ND 1.0 attenuator found necessary by Melfi with the original 24-inch receiver. The change in telescope required Northam and Brumfield to add a new detector package. Northam also initiated plans to evaluate the lidar in the calibration tank mode. Siviter assembled the calibration tank. The lead author then made contributions to the reliability of photon counting, the efficiency of detection, the certainty of specific pollutant detection, the flexibility of the data acquisition system, formulation of data analysis programs, and direction of the tests reported here. The photon counting and other detector contributions are outlined in Appendix 2. Efficiency of detection was improved by addition of the high

efficiency RCA 31034 photomultipliers, the acquiring of new, hybrid filter elements, and by the addition of provisions to tilt the interference filters to their peak transmission. The filters were carefully specified to be centered slightly above their Raman wavelengths so that the tuning distance would be small. Certainty of detection was improved by means of this ability to tilt the filters and by means of the hybrid filter combinations. The flexibility of the DAQ was improved by a hardware change to allow a dual (but interleaved) channel mode (ref. 15). Diagnostic and data analysis programs were formulated and appear in Appendix 1. The results to be presented in section 5 were directed by the lead author. Several changes in the LaRC lidar would have improved its performance still further, but time was not available to do both the demanding evaluation of the lidar at the calibration tank and the changes. These changes include an analog DAQ for daytime operation, better beam splitters to aid in selection and blocking, and the possible use of a doubled-frequency, high-repetition-rate YAG laser.

3C. Performance Predictions

The theoretical performance of the LaRC Raman lidar can be estimated on the basis of equation (4) and the parameters in tables 4 and 5 assuming that interferences have been eliminated. The questions of systematic error and calibration are discussed below. Table 6 summarizes this predicted performance. When viewing 1000 ppm SO_2 at 300 m, the return signal should be 0.55 counts per laser firing as registered by the DAQ in a 40-nsec bin (i.e., 6 m). The accumulation of 100 counts should enable a measurement of SO_2 in the calibration tank at night to a precision of 10% (i.e., a signal-to-noise ratio of 10). Such an accumulation would require about 200 laser firings or about 7 min. The potential for SO_2 monitoring at stacks is very promising.

Diagnosis of correct operation and of freedom from interferences of the Raman lidar involves the measurement of other

Table 6. Performance Prediction for LaRC Raman Lidar for Various Gases. Systems parameters are listed in table 5 and include a 6-m range interval at 300 m at a firing rate of 30 ppmin.

Gas	Concentration (ppm)	Time Period for 10% Measure (min)	Return per Shot (cts)	Remarks
SO_2	10^3	7	0.55	--
NO	10^3	83	0.04	--
CO_2(7683)	330	76	0.044	--
CO_2(7683)	3×10^4	--	--	--
O_2	2.1×10^5	--	1.23	ND 1.3 added
N_2	7.9×10^5	--	0.72	Other channel ND 1.0, etc.

gases in addition to SO_2. Table 6 contains entries for the predicted performance of the Raman lidar when viewing SO_2, NO, ambient CO_2, high concentration CO_2, ambient O_2, and, in the reference channel, ambient N_2. The N_2 counts are somewhat arbitrary depending on the configuration of the reference channel except that the 45 Mcps random count rate limit of the DAQ cannot be exceeded. Ambient O_2 operation is similar to the SO_2 operation except for the change of the spectral filter and attenuation to keep the count rate below saturation. The configuration of each type of operation is outlined in conjunction with the discussion of the channel transmissions and efficiencies appearing in table 7.

3D. Review of Raman Lidars Used for Stack Plume Measurements

A brief review is given here of all the Raman lidars used for stack plume or other pollutant gas measurements that have been described in the open literature as of the date of this report. Table 8 is a summary of this review. Assuming that the interference problem and lidar calibration have been successfully handled, the most important column for the purposes of comparing various lidar is the performance column. The measure of performance used here is the time period needed to make a measurement to a particular precision. This performance time period is here determined by scaling the reported results of the various lidar groups to the hypothetical measurement of 1000 ppm SO_2 at a distance of 300 m with a precision of 10 percent. A range interval of 6 m has been used and the use of a standard size 8-inch receiver has been assumed. The other columns of table 8 identify the Raman lidars and give several of their distinguishing features.

As previously stated, Inaba and Kobayasi (ref. 7) first measured SO_2 in a nearby (30 m) oil smoke plume in 1970. Night measurements of SO_2 in a distant stack plume (200 m) were later reported by Nakahara et al.(ref. 14). These workers were much

Table 7. Transmissions and Efficiences of the Several Channels of the LaRC Raman Lidar. The lower half refers to the standard lamp class of operation and the upper to the Raman class of operation.

Parameter	SO_2	CO_2	O_2	N_2
ε_{RAM}	0.025	0.025	0.0013	0.00025
λ_{ratio}	0.91	0.93	0.94	1.0
τ_1^{RAM}	1	1	0.05	0.1
ε_{PMT}	0.16	0.16	0.16	0.037
τ_{tele}	0.5	0.5	0.5	0.5
τ_{BS}	0.95	0.95	0.95	0.7 (?)
τ_{atm}*	0.9	0.9	0.9	0.9
τ_{schott}(5 mm)	0.58	0.61	0.63	0.46 (10 mm)
$\tau(p)_{filter}$	0.66	0.64	0.69	0.51
λ FWHM (Å)	27	27	28	17
$\tau_{\|\|}^{pol}$	0.84/2	0.84/2	0.84/2	0.88/2**
τ_1^{sl}	0.005	0.005	0.005	0.01
ε_{sl}	5.8×10^{-5}	6.0×10^{-5}	6.2×10^{-5}	1.1×10^{-5}

* One way transmission over 300 m.

** Depends on particular beamsplitter combination. Here leakage "adds" 1.05 factor.

Table 8. Summary and Comparison of the Performances of the Several Raman Lidars Used for Pollution Monitoring. Performance numbers are scaled from actual reports to a hypothetical measurement of 1000 ppm SO_2 at 300 m with a common 8-inch telescope.

Group	Date	Performance	Remarks	Reference
Inaba and Kobayasi	1970	400 min	6943 and 3371, spectrometer, plume at 30 m	6,7
Nakahara et al.	1972	40 min	5320, filters, stack at 200 m	14
Leonard	1972	33 min	3371, spectrometer, jet engine	20
Hirschfeld et al.	1973	2.5 min	3472, spectrometer, daytime, gas clouds	21
DeLong	1974	1.5 min	3472, etc., gas clouds	22
Melfi et al.	1973	6 min	6943, filter, stack at 200 m	16,23
This paper	1975	15 min	6943, filters, cal. tank at 300 m	--
Kuper and Ebeling	--	120 min	6943, spectrometer, cal. tank at 50 m	24

more concerned with the demonstration of the technique and elimination of interferences than with performance although they did attempt an absolute lidar measurement. Their recommendations for the use of a high-repetition-rate, doubled-frequency (e.g., 5320 Å) YAG laser are somewhat altered today by the availability of efficient red photosurfaces and by NO_2 fluorescence (ref. 18) and aerosol fluorescence (ref. 19) in the green. Interference filters were used to select the SO_2 wavelength. The Japanese group also recognized the limitations of photon counting when a high background was present and when one had high instantaneous signal rates. Leonard (ref. 20) used Raman lidar to measure the composition and temperature of aircraft engine exhaust emissions. Among other features, he first used analog detection under computer control. Several descriptions of the Block Engineering lidar are available; see Schildkraut (ref. 10), Hirschfeld et al. (ref. 21), and Delong (ref. 22). This instrument is now based on a doubled-frequency ruby laser, a polychromator, and an analog detection system capable of daytime operation. It is probably the most powerful of all the Raman lidars due partly to its 36-inch receiver, but its complexity appears to limit its frequent use. Melfi et al. (ref. 16) used a Raman lidar based on the ruby laser and interference filters to measure SO_2 at a stack 200 m away. Melfi (ref. 23) indicates its larger telescope (i.e., 24-inch), but lower efficiency photodetectors, would place this lidar about a factor of two better in performance than the present LaRC lidar. However, Melfi et al. (ref. 16) state that the quoted performance was obtained with an ND 0.9 attenuator in the return beam so that there is a discrepancy of about 2 to 4 between their results and the returns predicted in table 6. It is possible that aerosol fluorescence might have caused this discrepancy (ref. 23).

In few of the above lidars was much attention paid to absolute performance. The reports contain very little information on which to base the performance estimates in table 8.

None of the above groups measured a known concentration of pollutant gas in a calibration facility although many tried to estimate by other means the plume concentration. Measurements of nearby, artificial pollutant clouds were made, but mainly from the point of view of demonstration of the Raman technique. The present report is the first describing measurements of known pollutant concentrations and possible interferences under controlled conditions.

3E. Possible Interferences

3E1. Introduction

The design of the Raman lidar must include means to separate the various spectral components in the scattered light and minimize possible interferences. Two types of interference must be guarded against: leakage of the wrong wavelength return or acceptance of natural or induced broad-band background light into the spectral bandwidth of a receiver channel. The leakage can be due to either an inadequate rejection ratio of the spectral selector for strong returns at other wavelengths or to overlaps of the rotational structure of a Raman line with the spectral band selected. The broad-band background light could be either day background or fluorescence induced by the illuminating light pulse from gases or aerosols. If fluorescence is present, one may also have to correct for the additional absorption of light in the stack plume as indicated in equation (4). If any of these items or the ones discussed in sections 3F and 3G are overlooked, the potential of Raman lidar summarized in table 5 cannot be achieved.

3E2. Filter Leakage Interference

Filter leakage interference can be due to inadequate rejection ratios for Raman returns far from the line selected or for returns close to the line. Each are treated differently. Leakage interference can also be due to an overlap of the rotational structure of a nearby strong line with the spectral band selected. One of

the most serious rejection problems is that of Mie scattered light from plume aerosols at the same wavelength as the exciting line. Mie backscatter from atmospheric aerosols and diffuse scatter from the tank apertures and backstop are the corresponding problem at the calibration tank. An estimate of the seriousness of Mie backscatter can be made by using some of the typical backscatter functions. In the lidar geometry of table 5, one would have an equivalent backscatter coefficient of 3×10^{-10} for Raman O_2 scatter, 2.4×10^{-6} for Rayleigh scatter, and 1×10^{-4} $ster^{-1}$ for a 10 km visual range ambient maritime aerosol. Assuming that the 3M black velvet paint on the backstop used in the tank tests is less than 0.5 percent reflecting, one can estimate its backscatter coefficient to be about 1.6×10^{-3} $ster^{-1}$. Backscatter from a stack plume might lie between that of the backstop and that from a white target with a value of about 0.3 $ster^{-1}$ depending on the opacity of the plume. These estimates show that the Mie backscatter must be blocked from entering the spectral selection device by a very large factor. That factor might range from 10^{12} to 10^{14}. The present Raman lidar makes use of interference filters (e.g., fig. 6) which are naturally suited to giving high transmission for the 7546 Å SO_2 line and good rejection against Mie backscatter at 6943 Å and N_2 Raman at 8283 Å. The present filters were selected for relatively sharp shoulders and high transmission. Narrower filters can be inserted in the optical channel if found necessary. Other lidars make use of spectrometers for the selection. These spectrometers have typically had excellent rejection ratios, but poorer transmissions. The use of spectrometers becomes attractive for lidars using lasers toward the UV where interference filters have poor transmissions and where lines are closely spaced (e.g., SO_2 at 3852 Å and CO_2 at 3600 Å). The rejection ratios of both filters and spectrometers can be augmented by the use of absorbing glass filters. Figure 7 shows the transmission of a piece of Schott RGN-9 color glass used in the present lidar. A series of these glass filters with different thicknesses were obtained in order to optimize and study the

blocking of the Mie backscatter light at 6943 Å. Tests of the efficacy of the blocking were carried out by observing the return from the backstop during the measurements at the calibration tank, and by observing returns from artificial plumes. Additional rejection capability without a serious transmission loss is probably best added to a filter Raman lidar by means of special beamsplitters used at low angles of incidence to obtain sharp shoulders in their transmission curves (e.g., fig. 8). One would transmit the weak return while reflecting the strong reference. The Raman lidar described here does not have such beamsplitters. Other strong returns distant from the selected line may break through the interference filter in addition to the strong Mie backscatter. Figure 6 indicates that the N_2 return at 8283 Å is also naturally blocked, but that blocking at longer wavelengths may be a problem (e.g., water vapor at 9300 Å). The latter blocking can often be accomplished by taking advantage of the cut-off response of the photosurface used in the receiver. Figure 9 indicates several of these cut-off wavelengths. Use of a photosurface yields much higher net sensitivity on-line than use of metal films to block out longer wavelengths. Note that the C31034 photomultiplier used in the present lidar is not sensitive to the water vapor line.

Leakage of light through a filter due to a nearby Raman line (e.g., O_2 or CO_2 for SO_2 work) depends on the design of the interference filter. Raman excitation at 6943 Å is an advantage in that the Raman lines are well-spaced. This spacing allows one to use somewhat wider filters which have both good peak transmissions and sharp shoulders. The width also minimizes the temperature dependence of the peak wavelength of the filter. The dependence of the peak wavelength on angle of incidence (ref. 25) is made use of in this lidar to peak the transmission and to verify that one is in fact viewing a Raman line rather than a broad-band return. Blocking of nearby returns depends on the sharpness of the shoulders of the filters. Figure 10 shows a typical transmission curve of a three-cavity design,

all-dielectric filter which is currently available (ref. 26). For example, one can estimate the leakage through a 7683 Å CO_2 filter due to the 7784 Å O_2 Raman line. Figure 10 indicates that a blocking of 2×10^4 might be expected 100 Å from the CO_2 line center. Leakage at the 10 ppm level of CO_2 might then be expected. Section 5D presents measurements of ambient CO_2 which are relevant to this leakage question. On the basis of section 5D, an SO_2 filter can be expected to block the O_2 Raman return to the 2 ppm level of SO_2. Potentially more serious in an SO_2 measurement is the possibility of leakage due to the 7624 Å CO_2 line since the CO_2 in a plume can reach 10 to 20% levels. Figure 10 again indicates that leakage of Q-branch CO_2 scatter from 10^5 ppm CO_2 in a plume is not serious (e.g., 20 ppm of SO_2 contribution).

Raman scatter, however, is not confined to a single line (i.e., the Q-branch) as is indicated in figure 11 for scatter from nitrogen. About 12% of the scattered light in the parallel polarization is distributed in branches due to rotational structure of the line. It might be possible for this weaker scatter closer to the filter pass band to contribute to the lidar return. If one assumes that the CO_2 structure is the same as N_2 for the sake of an order of magnitude estimate, one finds that convolution of figures 10 and 11 indicates only a 10 ppm contribution of 10^5 ppm CO_2 to 10^3 ppm SO_2 in a stack plume measurement. Similarly, one can estimate that the O_2 branches do not contribute to a CO_2 signal at the 330 ppm CO_2 level. In view of the lack of explicit information about the CO_2 rotational structure and the uncertainty in the filter blocking for nearby wavelengths, it was decided to check for this type of leakage by viewing the calibration tank using the SO_2 filter when the CO_2 concentration was raised to 10^5 ppm. Section 5G presents the results of this test.

3E3. Broad-Band Background and Fluorescence Interference

Two types of broad-band background can obscure the Raman signal; natural background and induced fluorescence background. This interference can be minimized by proper spatial and spectral fil-

tering. Once minimized, it can often be eliminated by suitable data recording and analysis techniques. Total elimination of day background is possible by working at night. Total elimination of fluorescence is not possible unless a lidar wavelength can be selected that will not excite fluorescence. During tests with the Raman lidar at the calibration tank, it was found that day background rates were about ten times the standard lamp rates while looking at the black backstop. Measurements of N_2 and O_2 Raman returns were found possible under these conditions if the day background remained constant and was subtracted by additional measurements. Operation of the sensitive SO_2 channel would not be possible, however, because the day background rate of about 90 Mcps saturated the photon counting system. This saturation made data recording and subsequent background subtraction impossible. An analog data system would not be so limited (ref. 21). Induced fluorescence, if present, could also be subtracted from an observed signal. In this case, one would view the return at the selected line and at a line position nearby where no Raman return would be expected. A third channel could be used or a consecutive viewing period with the Raman line filter tilted so that it accepted only the dummy line. Again, one must minimize the fluorescence so that the photon counting system can record it. Induced fluorescence is known to be a problem at wavelengths shorter than 6943 Å with respect to both gases and aerosols (refs. 18, 19, 27). Little work has been done on this question at 6943 Å. Melfi et al. (ref. 16) conclude that they observed no fluorescence based on the fact that no decay time on the scale of 250 nsec was observed. They did not detune the filter, though, and a fluorescence decay time of less than 250 nsec might have been present. No estimates of fluorescence interference are made here. Attempts to measure its importance are described in sections 5I and 5H in the context of the calibration tank. Definitive tests will have to be carried out at a real stack plume. There one can employ at least three methods to identify fluorescence. The filters can be detuned to look for broad-band fluorescence, the range intervals can be narrowed to identify decay time constants as

short as 60 nsec, and, in the case of aerosols, the stack precipitators can be used to vary the amount of aerosols independently of the gases.

3F. Tests for Correct Operation

Tests for correct operation of the lidar typically consist of viewing a standard lamp placed at the range interval of interest and measuring N_2 and O_2 profiles through the atmosphere. These tests insure that the lidar data system is working correctly and that all optical elements of the lidar are in good condition. Correct operation of the data system means that the photomultiplier plateau has been reached, that the photomultiplier gate is properly adjusted, that multiple pulsing at the discriminator is not present, that noise does not enter the system during laser firing, and that the count rate saturation values are known and worked within. The first three questions as well as other photomultiplier related questions are discussed in Appendix 2. The latter two questions are discussed in sections 5A and 5B.

The optical performance of the Raman lidar can be checked by measuring an N_2 or O_2 profile in the atmosphere. However, it is just as effective and somewhat easier to view a standard lamp placed down range. Furthermore, the standard lamp can be used to diagnose any efficiency loss that might be noted in the N_2 tests. The predictions of Raman lidar performance in table 5 were not entirely achieved. The search for the discrepancy using the standard lamp is discussed in section 5E. The lamp used was a 1000 W GE DXW Quartzline lamp with a nominal spectral flux density at 7500 Å of 23 $\mu W/cm^2$ nm at 50 cm (ref. 28). The photon flux falling on the 8-inch aperture telescope at 300 m is approximately 9×10^9 photons per sec-Å and is denoted by B. The photon flux at 8283 Å is greater by 1.04. The count rates expected from the standard lamp in each channel are given by

$$R = \varepsilon_{s\ell} B \tau \int \tau_{filt} \, d\lambda \qquad (5)$$

where it is assumed that B and the system efficiency ε are constant over the small spectral width of the filter. The normalized spectral width of the filter is given by τ_{filt} which for estimation purposes is just the full-width half maximum of the filter in Å. The final factor, τ, represents any attenuation added which is not normally used. The system efficiency can be expressed as

$$\varepsilon_{s\ell} = \tau_{atm}\,\tau_{tele}\,\tau_{BS}\,\tau_{Schott}\,\tau_{pol}\,\tau_{p}\,\varepsilon_{PMT}\,\tau_{1} \qquad (6)$$

where τ_{atm} represents the transmissivity of the atmosphere from the lamp, τ_{tele} represents the transmission of the telescope, τ_{BS} represents the transmission (or reflectivity) of the beam splitter for the polarization in use, τ_{pol} represents the transmission of the polarizer, τ_{Schott} represents the transmission of the blocking filters, τ_{p} represents the peak transmission of the spectral filter, ε_{PMT} represents the quantum efficiency of the photomultiplier, and τ_{1} represents the transmission of any other optical attenuator normally used in the optical train. All of these transmissions and efficiencies were measured at either the wavelength of operation or one close by. Filter transmissions and shapes were measured on a Cary 17 spectrophotometer. Photomultiplier efficiencies were measured using the photomultiplier as a diode, an HeNe laser, a laser power meter, and the relative sensitivity curves of the photosurface. All of these parameters were determined in conjunction with the absolute efficiency search described in section 5E and are listed in table 8. The parameters in this table are arranged so that the components of the efficiency for Raman operation can be found by reading up from the lower dashed line and the components of the efficiency for standard lamp operation can be found by reading down from the upper dashed line. Table 9 lists the expected standard lamp rates for the parameters of table 8. Note the slight correction for polarizer leakage in standard lamp operation. Section 5E compares these predictions with actual measurements and discusses any discrepancies.

Table 9. Predicted Rates in the Several Channels of the Raman Lidar Viewing the Standard Lamp.

Channel	Rate (Mcps)
SO_2	14
CO_2	15
O_2	16
N_2	1.9

The standard lamp also aids in the optical alignment of the lidar. Using it, one can position the collimating lens and the lens that focuses the light on the small photosurface of the RCA C31034. One can also check for vignetting by moving the lamp through the field of view of the telescope. Auxiliary spectral lamps placed close to the telescope were also used. These were an independent check on the angle-tuning constants of each filter and on the location of the peak transmission wavelength.

3G. Calibration

The difficulty of making an absolute lidar measurement makes it imperative that a suitable calibration method be developed. Many workers have suggested using a second reference channel, usually N_2, to aid in this calibration. The concentration of the unknown gas can then be written in terms of ratios of known or measurable quantities. For example, the ratio of N_2 to O_2 concentration can be written as

$$\frac{n_{N_2}}{n_{O_2}} = \left(\frac{\lambda_{O_2}}{\lambda_{N_2}}\right)\left(\frac{\sigma_{O_2}}{\sigma_{N_2}}\right)\left(\frac{\varepsilon_{O_2}}{\varepsilon_{N_2}}\right)_{Ram}\left(\frac{\tau_3}{\tau_4}\right)\left(\frac{N_{N_2}}{N_{O_2}}\right) \tag{7}$$

where the wavelength ratios are given in table 8, the cross section ratios in table 4, the efficiency ratio is determined by the standard

lamp measurement, and the transmissivity ratio accounts for any optical attenuation added to or removed from individual channels for Raman operation if different than for standard lamp operation. The final factor is the ratio of observed range interval counts corrected if need be for pileup. It is here assumed that the filters are peaked for each Raman line. It is obvious that all the ratios in equation (7) are known except for the relative efficiency of the two channels. Similarly, any other gas concentration can be determined relative to N_2 using equation (7) as long as relevant relative efficiences can be determined.

The determination of the relative sensitivity of the two channels can be done in several ways. Measurement of the N_2/O_2 ratio in the atmosphere (i.e., 3.7) could serve to measure the efficiency ratio at these two wavelengths in addition to determining atmospheric and plume transmissivities and to providing laser pulse energy normalization. If the Raman line of the unknown concentration gas is close to the O_2 line, no further measurements would be necessary for calibration. In fact, one may wish to measure the ratio of unknown to O_2 as reference in this particular case. If the measurements are consecutive in time with a single channel, no linking of channels would be necessary. If done simultaneously in a dual channel mode, the two channels must be linked using Raman O_2 measurements in both. If the Raman line of the unknown gas is far from the O_2 line, the spectral gap must be bridged by use of the standard lamp. Either of the two reference methods outlined above could be used. Work in this report emphasized the use of the standard lamp and the N_2/O_2 ratio calibration methods. Most of the results quoted in section 5 were obtained with standard lamp calibrations. A number of these results were recalculated using the N_2/O_2 method as quoted in section 5I.

The relative Raman efficiences can be obtained from the relative standard lamp efficiencies using equation (5)

$$\frac{\varepsilon_{s\ell}^{O_2}}{\varepsilon_{s\ell}^{N_2}} = \left(\frac{R_{O_2}}{R_{N_2}}\right)\left(\frac{B_{N_2}}{B_{O_2}}\right)\left(\frac{\int \tau_{filt}^{N_2}\, d\lambda}{\int \tau_{filt}^{O_2}\, d\lambda}\right) \tag{8}$$

and using equation (6)

$$\varepsilon_{RAM} = \varepsilon_{s\ell}\ \tau_{atm}/\tau_{pol}\ \ \tau_1 \tag{9}$$

The most convenient form of the relative Raman efficiency formula is

$$\frac{\varepsilon_{RAM}^{O_2}}{\varepsilon_{RAM}^{N_2}} = \left(\frac{R_{O_2}}{R_{N_2}}\right)\left(\frac{B_{N_2}}{B_{O_2}}\right)\left(\frac{a_{N_2}}{a_{O_2}}\right)\left(\frac{\tau_p^{O_2}}{\tau_p^{N_2}}\right)\left(1.05\ \frac{\tau_{pol}^{N_2}}{\tau_{pol}^{O_2}}\right) \tag{10}$$

where the peak transmission of the filters allow the use of a, the ratio of filter areas as determined by weighing. If the polarizer is used for Raman measurements, only the 1.05 factor remains for N_2 reference measurements. Otherwise, the full factor must be used for N_2 reference measurements. O_2 reference work would not have this correction factor. The subscripts of equation (10) must be changed to correspond to the actual case at hand. The two basic calibration formulas are equation (7) and equation (10).

The relative calibrations just discussed yield absolute concentrations of pollutants to a precision determined by the length of time available to fire the laser. A loss of efficiency in a channel will not affect the ability to make the measurement, but only the time it will take to obtain enough returns to get the desired precision. The optimization of system efficiency is discussed in sections 3F and 5E. The accuracy of the measurement depends on the calibration procedure. A measure of the

lidar accuracy can be obtained by comparing lidar measurements of known concentration pollutants in the calibration tank with in situ measurements. These measurements are reported in section 5.

4. CALIBRATION TANK

4A. General

A Raman lidar calibration facility has been constructed to contain the gases for the calibration measurements. The tank consists basically of a steel tube 2 m in diameter and 20 m long. In principle of operation, the tank is charged with a quantity of gas which is mixed with ambient air to a known concentration. Raman lidar measurements can then be made through a known volume and concentration of gas.

4B. Tank Description

The calibration tank consists of a 2-m-diameter by 20-m-long steel tube. The tank is charged with gas through a 15-m-long perforated manifold. Two fans, located in the tank, are used to mix the charge. At each end of the gas tank there is an aperture 0.6 m in diameter. The aperture is required to maintain the gas mixture in the tank. A larger diameter aperture or no aperture would greatly reduce the gas residence time in the tank. Each aperture is fitted with a remotely operated shutter. The shutters are closed during short periods when measurements are not being made, thus increasing the gas residence time. A 1.3-m-wide air curtain fan is located at each end of the tank. Any outside air currents blowing down the tank would result in a loss of the gas charge in the tank. The heating and cooling system is used to regulate temperature and for dehumidification. This capability has been used primarily, to date, to dry the system for use with SO_2. Figure 12 is a schematic of the tank showing its principal components.

4C. Gas Operation

The tank has been operated for Raman lidar calibrations with various concentrations of CO_2 and SO_2. Gas mixtures have been maintained to within ± 5 percent of a desired level for residence times of 10 minutes. The tank has also been charged with varying concentrations of CO without difficulty.

4D. Aerosol Operation

Aerosol screens have been produced in front of the tank to simulate a smoke stack plume. The aerosol screens were produced by burning a mixture of used automotive engine oil and varsol. A waste cotton material was used as a wick-base for the smudge pot technique. The smoke was then vented through the air curtain fan to produce a screen of aerosols about 1.3 m wide by 15 cm thick.

4E. Instrumentation

The calibration tank instrumentation (table 10) consists primarily of gas analysis and temperature measurement. The handling of the gas sample for analysis is made with an Environmetrics gas handling pump. The gas sample is taken about mid-way in the tank through 6-mm-diameter teflon tubing. The sample is then pumped through the analyzer at a rate of about 1 to 3 standard cubic feet per hour. A chart recorder is used to record the gas concentration with time. Figure 13 shows a typical time history of the gas concentration for a CO_2 and an SO_2 run.

Table 10. Gas Sampling Instrumentation

Gas	Manufacturer	Range
CO	MSI LIRA	0 to 1000 ppm
CO_2	MSI LIRA	0 to 20%
SO_2	Environmetrics	0 to 5000 ppm

5. LIDAR MEASUREMENTS OF AMBIENT GASES AND HIGH CONCENTRATION POLLUTANTS IN THE CALIBRATION TANK

5A. N_2/O_2 Ratios in the Atmosphere

Measurements of the N_2/O_2 concentration ratios serve to check for correct operation of the lidar, calibrate the lidar for absolute measurements of pollutants, and to measure the atmospheric extinction. Initial measurements with the LaRC Raman lidar during these tests were concerned with the check for correct operation. The latter two possibilities were pursued during measurements through the tank. Figure 14 is a display of an early return from the atmosphere alone. The counts in each bin of the sixteen-bin photon counting system accumulated after a number of laser-firings were displayed here after the range square correction of equation (4) was made. The error bars on each point are statistical precisions. The N_2 and O_2 profiles were obtained consecutively since the sixteen bins form only a single channel. Range bins of 200 nsec were used for a total range time of 3.55 μsec or 511 m. The returns for each gas should show an exponential decay depending on the amount of extinction present. The scales are arbitrary in that the returns were attenuated to make them about equal and to place the initial count rates within the limits of the photon counting system. Figure 14 indicates that the fields of view of receiver and transmitter do not overlap until about 1.55 μsec for the receiver field of view used for this run. Not so obvious is the need for a pileup correction at the beginning of the profile to account for the random count limitations of the photon counting system (e.g., 45 Mcps). Figure 15 shows the ratio of the above profiles. The units are again arbitrary along the abscissa since the relative sensitivity of the two channels is not known without additional information. Note that the adjustment of both returns to about the same value in figure 14 corrects for much of the overlap and pileup problems without explicit calculation. The ratio curve in figure 15 should be a straight line with range. Appendix 1

compiles the data analysis programs that allow presentations of data and results such as in figure 14 and figure 15 along with the various corrections (e.g., pileup).

5B. N_2/O_2 Ratios Through the Calibration Tank

Most of the Raman lidar work was done in conjunction with the calibration tank. Initial N_2/O_2 profiles and ratios were taken to verify that backscatter from the tank and tank apertures would not break through the blocking into the Raman channels. Elimination of this backscatter was found to be necessary for the highest sensitivity channel. It was accomplished by proper configuration and blackening of the tank and by proper choice of auxiliary blocking filters. Figure 16 shows the atmospheric profiles through the tank on the same range scale as figure 14. The profile is truncated by the backstop that was placed to make the lidar range safe to passers-by. Note that the nitrogen channel shows no sign of the backstop whereas the oxygen channel shows its presence. The oxygen channel is obviously poor in blocking the Mie scatter from the backstop even though a 5-mm Schott filter was used. The interference filters in this test were soon replaced with new filters. Neither channel indicates the presence of the tank which normally appears about 1.9 μsec. It was found that apertures as small as two feet in diameter could be used to help contain gas in the tank as long as the laser beam was collimated to 1 millirad in full width, the tank apertures were kept smooth, and kept black with 3M Black Velvet paint. Tests with the highest sensitivity channel are discussed in sections 5D and 5E. The residual counts after the backstop in figure 16 are due to afterpulsing in the photomultiplier which is discussed in Appendix 2. Both tubes were RCA 8852 at this time.

Once it was proven that the Raman lidar could look through the tank successfully, attention was placed on the atmospheric profiles again for purposes of exploring the calibration of the lidar and measuring atmospheric extinction. Figure 17 displays

sample returns from the atmosphere through the tank. The time bins are now 40 nsec which allows two bins to be placed within the tank as discussed in section 5C. Figure 17 shows no evidence of tank breakthrough. The backstop is just out of range. Figure 18 shows the N_2/O_2 count ratio accompanied by an absolute scale determined by standard lamp measurements. The observed ratio of 3.8 ± 0.1 indicates fair agreement within the expected 3.7. It is typical of N_2/O_2 profiles. This calibration proceeded as discussed in section 3G with the properties of the interference filters known by laboratory measurements and with their peaks adjusted to the Raman line wavelengths empirically by tilting. Standard lamp ratios were first taken with an auxiliary counter connected to the photon counting system. This method was later replaced by taking the calibration data with the complete system itself (triggered by an auxiliary pulser) and by analyzing it in a manner similar to the profile ratios as discussed in Appendix 1. Such a standard lamp profile is a good check on correct operation of the detector. The fluctuation of the data points in each bin of figure 17 raises questions concerning the true width of the time bins, the true randomness of the counts, and the possibility of noise during laser firing. The latter is the most difficult question to answer due to the low Raman return. It was eliminated by observing the standard lamp through a SO_2 filter with no SO_2 gas present and with the laser firing out of the receiver field of view. The first two questions are closely intertwined. Extensive tests and analysis with the standard lamp showed that fluctuations such as appear in figure 17 are normal and that the widths of the bins were correct to a few percent.

5C. High Concentration CO_2

The encouraging results with the Raman lidar for atmospheric constituents prompted measurements of other gases in the calibration tank. CO_2 was chosen because it is not toxic like SO_2. A range of concentrations was chosen that spanned a return signal as small as that from 1000 ppm SO_2 up to ten times that signal.

The CO_2 concentrations ranged from 10,000 to 35,000 ppm. Figure 19 shows the CO_2 profile and the N_2 reference profile. The CO_2 return was taken with the more sensitive RCA 31034. The channels were taken consecutively in time. The time scale of operation (e.g., 100 shots) does not allow the ambient 330 ppm CO_2 to be seen. Operation of the CO_2 channel without CO_2 in the tank is a good means to monitor the condition of the black surfaces of the tank and any resultant increase in Mie backscatter breakthrough from the tank. Routine use of this test is time-consuming, however, so it was replaced by an analog Mie detector installed as a third channel in the Raman lidar detector package. Tank Mie returns were typically 0.01 times the backstop return. To obtain absolute CO_2 concentrations from the lidar measurements shown in figure 19, the standard lamp calibration method was again used. Figure 20 compares the Raman lidar measurements of the various CO_2 concentrations with the concentrations measured by the in situ gas sampler. The systematic error appears to be smaller than about 10 percent. Similar results were obtained during several other high concentration CO_2 tests. The Raman lidar could thus be used to characterize the high CO_2 concentrations in a stack plume if those were of interest (ref. 23). These results with CO_2 indicated that the Raman lidar, the calibration tank, and the lidar calibration method were ready for the more demanding measurements of 500 ppm SO_2. The absolute return of the 19 December 1974 test corresponded to 0.7 counts/shot which is a factor of 3.4 lower than predicted by table 6 once the presence of a second 5-mm Schott filter in the CO_2 was taken into account. The standard lamp CO_2 rate was 5.8 MHz which is a factor of 1.6 smaller than predicted by table 9 once the extra Schott filter is taken into account. These discrepancies in absolute return and performance instituted a lost photon hunt which is summarized below in section 5E.

5D. Ambient CO_2

Table 6 indicates that a Raman lidar capable of detection and measurement of ambient CO_2 at 330 ppm should certainly be capable of measuring 500 to 1000 ppm of SO_2 as long as interferences are

not present. The time period for such a measurement would be twelve times that for the SO_2 measurement or a predicted 76 minutes. In view of this long period and the capability of placing known concentrations of gases in the calibration tank, no work was done specifically on ambient CO_2. However, in the course of the high concentration CO_2 measurements, signals from ambient CO_2 were obtained from those time bins outside the tank. These signals imply that the ambient CO_2 concentration was 850 (± 170) ppm which is much too high unless leakage of CO_2 from the tank raised the concentration to that value temporarily. Assuming that gas leakage from the tank could not cause such a high reading, one can set an upper limit for the blocking of the CO_2 filter to O_2 Raman scatter. Mie backscatter is not expected since two 5-mm Schott filters were in use. The excess counts when attributed to O_2 Raman scatter indicate that the CO_2 filter blocking for the O_2 line (100 Å away) is only a factor of 1.4×10^3. Figure 10 indicated that one might have expected a blocking of 2×10^4. Narrower filters could be ordered to obtain a higher blocking if desired. Since the CO_2, O_2, and SO_2 filters are all very similar in peak wavelength and shape, one can estimate the blocking expected for these filters and other lines as discussed in section 3E. One should try two CO_2 filters in tandem to try to eliminate the leakage.

5E. Absolute Efficiency Search

The high concentration CO_2 results of December 1974 indicated that the standard lamp signal was low by a factor of 1.6 and the CO_2 Raman signal low by an additional factor of 2.1 from the predicted signals based on the parameters of table 7. The situation was not clear at the time because not all the system parameters were then as well known as implied in the discussion of table 7. The 3.4 discrepancy was serious since it made the difference between 6 min and 20 min in predicted performance. The search also took longer than might be expected because of modification of the single channel photon counting system to a dual channel

system, installation of gating provisions for the C31034 photomultiplier, studies of partial reduction in auxiliary blocking in the O_2 channel, and a variety of other changes and mishaps. During this time period, the extensive statistical tests were carried out. The particular C31034 in use from December 1974 to May 1975 probably degraded in use by a factor of two over this period and was, in fact, destroyed by accident on 2 May. A concurrent problem with the photomultiplier bias circuit also took place on 2 May. After installation of a new base and tube, the LaRC Raman lidar performed at its highest sensitivity. A N_2/O_2 profile on 16 May gave returns of 0.45 counts/shot for N_2 and 0.60 counts/shot for O_2. The standard lamp rates were 9.6 Mcps for O_2 and 1.4 Mcps for N_2. Comparisons to table 6 and table 9 indicate that the standard lamp rates are down by a factor of about 1.5 and the Raman rates are down by a factor of 1.3. The airfield visibility that night was reported as 6 miles in haze, clearing after a rain shower to 7 miles. The light rain that night did not appear to affect the Raman returns. The slope of the N_2 and O_2 Raman returns showed little evidence of any absorption due to the atmospheric conditions. One concludes that the discrepancies are real. Extensive tests of the receiver were carried out during which field of view, focusing, aberrations, photosurface scans, etc. were all studied. It is suggested that the receiver discrepancy of 1.5 may still be due to a poor telescope mirror reflectivity in the 7600 Å region in addition to the 50 percent transmission measured at 6328 Å. If this reflectivity is the sole cause of the receiver loss, the Raman return can be increased by a factor of 4 by recoating the mirrors. The discrepancy in the Raman rates by a factor of 1.3 cannot now be explained. It may be due just to uncertainty in one of the other transmissions or efficiences in table 7.

5F. SO_2 Measurements

During May to July, four observations of SO_2 concentrations in the calibration tank were made. Only two of these were made after peak performance of the lidar had been reached. Figure 21

shows the results of the analysis of the measurements of 19 May 1975. The range profile is not shown since it has all the same features as the CO_2 range profile in figure 19. Most of the data for 19 May was taken in the dual channel mode so that a simultaneous N_2 normalization profile was obtained. The cost of this could have been a systematic error due to the single SO_2 range interval not being centered in the tank. The numbers at each point in figure 21 are the number of laser firings needed to obtain that point with its corresponding precision. This result in addition to the other SO_2 runs is the basis for the conclusions of this paper that the LaRC Raman lidar is capable of night measurements to 10 percent accuracy of 1000 ppm SO_2 in stack plumes at a distance of 300 m if interferences are eliminated or accounted for.

In these tests, the SO_2 was certainly being detected because the signal except for a small residual disappeared when the gas was released from the tank. In addition, the SO_2 filter was detuned by tilting and the signal also disappeared.

5G. Gas Interferences

Several possible gas interferences with the measurements of the Raman lidar have been discussed in section 3E. One of these, O_2 Raman leakage through the CO_2 filter, was examined in section 5D above. That examination indicated that the inteference filters appeared to perform 20 times worse than the expected behavior given in figure 10, and led to estimates in section 3E of other leakage possibilities. For example, the O_2 Raman return should be blocked to the 2 ppm level when using the SO_2 filter. The stronger N_2 Raman signal should contribute even less. The closer CO_2 Raman line at 7624 Å was expected to contribute about 20 ppm to an SO_2 measurement if the CO_2 concentration was 10^5 ppm. Preliminary results of this CO_2 test of the SO_2 filter on 26 June 1975 was that the leakage signal could not be distinguished from leakage through the SO_2 filter in the absence of CO_2 in the tank. The background breakthrough of the SO_2 filter corresponded to 0.01 counts/shot or 40 ppm of SO_2. The cause of this leakage is

not known. The only other prevalent atmospheric constituent is water vapor, but the photomultiplier photosurface is not sensitive to its wavelength. One should try two SO_2 filters in tandem to help distinguish the cause of this leakage.

No tests of gas fluorescence were made other than the detuning of the SO_2 filter when SO_2 was in the tank. One may wish to test NO_2 for fluorescence leakage (since this is one noise source in the green, ref. 18) in spite of the fact that its concentration will be quite small right at the stack (tens of ppm).

5H. Particulate Interferences

Mie backscatter interferences and possible particle fluorescence interferences can affect the Raman lidar results as discussed in section 3E. Mie backscatter from stack aerosols is the possible problem at the stack. Mie backscatter from atmospheric aerosols and diffuse scatter from the tank apertures and backstop are the problem at the tank. The residual counts in the SO_2 Raman channel might be a problem of Mie backscatter from ambient aerosols. It will be of interest to check this hypothesis here by scaling from the observed backstop breakthrough signal using the estimated backscatter functions of section 3E3. Similar means to check and eliminate Mie backscatter would be used at a stack. A stack plume is not expected to be as an effective scatterer of light as a black (or white) target, especially with the present emission regulations. The observed return from the black backstop using the SO_2 filter and a 6-mm RGN-9 absorber is about the equivalent of 3×10^3 ppm SO_2. The tank is not usually seen under these conditions. Assuming that the black backstop is still less than 0.5% reflecting (ref. 29), one can estimate a return of about 150 ppm SO_2 for a typical aerosol breakthrough. A residual SO_2 signal of about 30 ppm SO_2 was observed. However, the analog channel showed that scatter from the tank apertures was of greater magnitude than aerosol scatter at the range of the tank so that the tank apertures should also have been seen in the residual SO_2 signal. Also, addition of an

extra 1 mm of RGN-9 did not eliminate the residual SO_2 return as it should have done.

Fluorescence of aerosols is a problem that can only be studied at a stack due to the difficulty of imitating the aerosols in a real plume. The authors found it difficult to produce a plume just for the purpose of checking the blocking that would be needed at a stack much less one for the study of fluorescence. At least another 5-mm RGN-9 Schott glass filter will be needed at a stack. It is possible that the residual SO_2 signal is due to ambient aerosol fluorescence.

5I. Alternate Calibration Schemes and Systematic Errors

The alternate calibration scheme to the use of a nitrogen reference channel is the use of an oxygen reference channel. Its advantage is its proximity in wavelength to the SO_2 Raman line. The spectral lamp need not span such a wide response region. In addition, the identical channel can be used with only the use of an auxiliary optical attenuator to keep the count rate comparable. Until the lidar is modified to have two identical channels, the method requires consecutive profiles. A test of this scheme directly has not yet been carried out due to other priorities and equipment difficulties. However, a number of both CO_2/N_2 and SO_2/N_2 measurements were made the same night as O_2/N_2 ratios. It was then possible to determine the SO_2 concentration, for example, in two ways. The nitrogen normalization technique plus standard lamp yielded 1130 ± 140 ppm. Use of the N_2/O_2 ratio in addition to the N_2/SO_2 ratio to obtain an absolute SO_2 concentration yielded 1150 ppm SO_2. The data run was number 7 of 19 May. The sampling indicated 1367 ± 257 ppm. The systematic error was not affected in this hybrid calibration technique. Whether or not the direct O_2 calibration would eliminate the systematic error is not obvious. A similar test with CO_2 data of 10 December 1974 indicated an increase from 76,000 ppm to 84,000 ppm using the O_2 hybrid scheme. The actual in situ CO_2 concentration was 74,000 ppm in this case. Most of the N_2/O_2

ratios were also high, again indicating a systematic error and a lower than expected O_2 concentration. The cause of this systematic error is not known.

6. LIDAR MEASUREMENTS OF AEROSOL PLUMES AND ATMOSPHERIC EXTINCTION AT THE CALIBRATION TANK

6A. Theory and Review of Other Lidar Measurements

Many workers have suggested the use of remote Raman scatter to obtain the transmittance of the atmosphere and aerosol plumes. Leonard and Caputo (ref. 30) have made the most thorough investigation of such possibilities experimentally for the atmosphere and artificial smoke clouds. In the present context, one would view the range dependence of the nitrogen Raman scatter at 8283 Å. Equation (4) indicates that this range dependence would lead to a measure of transmittance since the cross section and distribution of nitrogen is known. Figure 22 shows schematically such a return for many laser firings. The slope of the line depends on the atmospheric transmittance as in figure 17 and the discontinuity on the plume transmittance. The smoke plume transmiitance can thus be determined in principle as long as single scatter prevails and enough radiation traverses the plume. It is also assumed that there are no other absorbers present and that interferences such as fluorescences have been eliminated or accounted for. The principle of this transmittance determination using the Raman lidar is very similar to the lidar method tried by Cook et al. (ref. 31) using Mie scatter from ambient aerosol before and after the plume. The Raman scatter method has several potential advantages which will alleviate difficulties with the Mie scatter method.

For many purposes, knowledge of the atmospheric or plume transmission is sufficient. For example, a model for radiative transfer through the atmosphere including aerosols may only require the net transmittance to be measured. For plumes, one of the Federal Emission Standards (ref. 2) limits the opacity of the

plume to 20 percent or less except for 2-min periods every hour. The opacity measurement is also important for the proper interpretation of SO_2 measurements in the plume. Leonard and Caputo (ref. 30) measured cloud transmittance to several percent precision over a range of one-quarter mile. The potential for the LaRC Raman lidar for plume transmission measurements will be discussed below.

The second Federal Standard (ref. 2) for particulates in stack emissions requires the mass emission rate to be below 0.18 $g/Mcal_h$. Reference to table 1 indicates that s percent coal, for example, will emit 8.2 s $g/Mcal_h$ input. A plant burning one percent fly ash coal would therefore need a precipitator operating at 97.8 percent efficiency to enable the plant to meet the emission standards. Again, the standard is not written in terms of rates so that all plants must have the same efficiency precipitators and the larger plants can put a larger absolute amount of particulates into the air. The Federal Standards for emissions (ref. 2) specify the methods to be used to determine the mass emission rate of particulates. Due to difficulties of location, operation, etc. of these other devices, it is useful to raise the question of whether or not a transmissivity measurement could be interpreted in terms of a particulate mass emission rate. Conner (ref. 32) has reviewed this question as well as the various methods for measuring opacity and transmissivity of plumes. There is evidence in certain cases that opacity can be rather directly related to particulate mass concentration in a plume. This mass concentration must be related to mass emission rate by means of supplementary measurements of plume exit velocity and diameter.

Mie lidar measurements of stack plumes yield another parameter which depends on the aerosols and their concentrations. That parameter is the Mie backscatter coefficient, $\beta_A(\pi)$, which would replace the $n\sigma$ in equation (4). The lidar return, however, now depends on both $\beta_A(tot)$ and $\beta_A(\pi)$ and these cannot be determined exactly unless they can be otherwise related. Collis and

Uthe (ref. 33) address this problem and show how $\beta_A(\pi)$ can be approximated based on additional assumptions and/or measurements. One such measurement is just the transmission one already discussed. Another is to calculate the relationship based on particle size data obtained by sampling. Johnson and Uthe (ref. 34) obtained measures of plume (length-wise) mass content for a stationary source stack in this manner. A third method would be to find an empirical relationship between the backscatter coefficient and the opacity. Collis and Uthe (ref. 33) obtained encouraging results in a controlled scattering chamber with injected fly ash. They found indications that a lidar wavelength of 0.7 μm yielded results dependent on opacity whereas a wavelength of 1.06 μm yielded results more closely related to mass concentration. It is not clear that any of these aerosol backscatter measurements possess any advantage over the opacity measurement discussed in the prior paragraphs.

6B. Predicted Performance of the LaRC Raman Lidar

The LaRC Raman lidar can be used either in a single channel mode or in the dual channel mode to measure plume transmittance by recording the nitrogen signal as a function of range. Figure 22 displays schematically such a return. Note that the background atmospheric transmission is also measured as the slope of the general curve. The plume transmittance is measured by the discontinuity at the plume location. For estimation purposes, one can reduce the analysis to the data points from the range bin before and after the stack. The transmission of the plume can be written as

$$N_2/N_1 = T = e^{-\tau}$$

where N_2 and N_1 are the counts after and before the plume and τ is the two-way optical thickness of the plume. Assuming the absence or correction for systematic errors, one can express the error in the optical thickness as

$$\Delta\tau = \sqrt{(e^{\tau} + 1)}/\sqrt{N_1}$$

on the basis of random statistics of the received counts. The error in transmission can be expressed as

$$\Delta T = T\Delta\tau$$

Table 11 is a summary of the time periods expected for the stated number of total counts needed in the first bin to obtain 5 percent measures of high T and 10 percent measures of low T. It has been assumed that the N_2 channel attenuation has been adjusted to yield about 1 count/laser firing. Higher returns are handled with increasing difficulty by the photon counting DAQ. Night measurements are also assumed. Note that the time periods get long at both high transmissions and low transmissions. No improvement can be made with the LaRC lidar unless a high-repetition-rate laser is used with less attenuation (or a larger receiver) or unless an analog DAQ is installed with the same proviso. The latter case would allow day operation with proper choice of telescope size.

Possible interferences are fluorescence and inadequate blocking, both of which have been adequately treated in section 5. The advantage over the conventional lidar method of measuring transmission (e.g., Cook et al., ref. 31) is that the intense return from the plume is blocked before reaching the detector and does not cause overloading of the analog DAQ or afterpulsing of the photomultiplier. Both of these problems are serious for a conventional Mie lidar.

6C. Results

Several attempts to measure plume transmittance of fake plumes at the calibration tank during the interference studies were not successful due to the difficulty of producing the type of plume needed for the interference studies. It is recommended that the plume measurements be continued during a field trip to a stack.

Table 11. Time Periods Needed to Measure Various Plume Transmittance Using the LaRC Raman Lidar to View Nitrogen Raman Scatter. Returns in that channel have been adjusted to yield 1 count/shot in the interval before the plume.

Transmission T	Optical Depth τ	N_1 (counts)	Δτ	ΔT	Period (min)
0.90	0.1	1300	0.04	0.04	43
0.82	0.2	900	0.05	0.04	30
0.37	1.0	400	0.1	0.04	13
0.13	2.0	600	0.1	0.013	20

Monitoring of atmospheric transmission was quite difficult due to the short baselines involved for both Raman and standard lamp measurements and due to the low aerosol attenuations. Over the period 18 December 1974 to 10 July 1975 many nitrogen profiles were obtained. They showed a general correlation with the highest lamp rates (e.g., 1.7 Mcps) corresponding to flat range-squared nitrogen profiles and with the lowest lamp rates (e.g., 1.52 Mcps) corresponding to Mie attenuation coefficients of 0.5 Km^{-1}. The standard lamp extinction over 300 m is not inconsistent with such a coefficient (e.g., 0.86). The two-way Raman extinction would be 0.75 for the worst case. The typical Mie coefficient for the nights of operation was 0.25 Km^{-1} or 0.86 two-way Raman extinction. The extinction of the nitrogen profile in figure 17 was also the greater value, but did not fit into the above sequence due to the use of a different lamp. Kildal and Byer (ref. 12) quote a Mie extinction coefficient of 0.24 Km^{-1} for visibilities of 10 km maritime haze. Visibilities in the visible obtained from the nearby airfield were 7 to 10 miles on several of these typical nights. These visual visibilities were determined by observers in the flight tower as they looked at nearby features. Both observer and feature were probably above the ground haze which was common on the marshy lidar range in early evening. None of the measures of Raman return or standard lamp rates were taken for the express purpose of determining atmospheric extinction. They are therefore not accurate enough for determining the low extinctions that were typical of the nights of operation. Closer attention to the measurement would greatly decrease the errors and provide a more accurate measure of atmospheric extinction.

7. CONCLUSIONS AND RECOMMENDATIONS

The tests of the LaRC Raman lidar at the calibration tank at a distance of 300 m indicate that night measurements of SO_2 concentrations in stack plumes are possible. Accuracies of 10 percent are achievable within 30 min integration times for 500 ppm

of SO_2 at the stack exit. Comparable measurements of HCl at a rubbish-fueled stack should also be possible. Supplementary measurements are required to obtain the concentration and mass emission rate. The possible interference of aerosol fluorescence can only be evaluated at a real stack. If fluorescence is present, it can be subtracted from the signal as long as reasonable signal-to-noise ratios exist. Simultaneous measurements of plume transmission are possible with this dual-channel lidar. Accuracies of better than 10 percent in transmission of the aerosol plumes should be possible within 30 min with the LaRC lidar. An early test at an instrumented stack is strongly recommended.

The time period for the above measurements can be decreased somewhat by improving the telescope transmission and finding the source of the absolute discrepancy with predictions. With the present lidar and photon counting DAQ, these time periods can be decreased by about a factor of 4 until the bin count rates approach random count saturation. A larger telescope or larger laser pulse energy would not help once this saturation rate is exceeded. For night operation, a high repetition-rate laser at the same or higher average power in conjunction with a larger telescope would decrease the time periods of observation even more. The high repetition rate Nd:YAG laser is known to excite the fluorescence, however. To make day operation possible, one really needs to have the combination of a somewhat larger telescope and a laser pulse of higher energy. The present lidar with its efficiency discrepancies eliminated should be capable of day operation if an analog DAQ were added in the several channels. The analog DAQ should possess the capability of the same 20 to 40 nsec time-bin operation. Analog operation would also aid the plume transmittance measurements since these rates were artificially lowered in the present lidar and aid the discrimination against fluorescence. If the new DAQ were added, one may also want to consider the use of an O_2 reference channel rather than an N_2 channel and make both channels identical. The size of the lidar van prevented this step in the present lidar. The advantages of the O_2 reference

are that one does not need a special beamsplitter (a piece of glass will do) and the spectral distance between the SO_2 line and the O_2 line is quite small, making standard lamp calibration more reliable. In HCl operation, one would still use the N_2 reference channel.

In conclusion, the present lidar is an adequate instrument for monitoring SO_2 and plume opacity from stationary sources at night. Its large depth of field is a definite plus. Its compact size and ease of maintenance and operation compare favorably with larger, spectrometer-based Raman lidars. The N_2 channel maintained its performance over the whole year of operation. Its photon counting system makes possible this small size and provides very modest but adequate data-recording capabilities. That photon counting system also restricts the lidar to night operation. An analog DAQ added to the present lidar in addition to the improvement of receiver efficiency should provide a powerful device for the remote measurement of SO_2 and HCl stationary source emissions at the 500 ppm level and for the measurement of plume transmissivities during day and night.

ACKNOWLEDGEMENTS

The success of the Raman lidar work is the net result of the contributions of many people. The history of the lidar up to the time the lead author arrived is outlined in section 3D. I would like to thank G.B. Northam for providing the opportunity to do this work and for his support and encouragement during my two-year sojourn at NASA-Langley Research Center. In addition to the co-authors of this report, I would like to acknowledge the assistance of Ellis Remsberg, Ed Browell, Carolyn Jones, Chet Bartusek, Jane Cissell, Spence Inge, and E.M. Maygarden, I want to make special mention of the many contributions of Lloyd Overbay to the success of the Raman lidar work. Finally, I would like to thank all those at Old Dominion University whose good offices allowed this sojourn and all those in higher level positions at NASA Langley who supported me during this sojourn.

REFERENCES

1. Williamson, S.J. "Fundamentals of Air Pollution", Chapters 7, 8, and 9, Addison-Wesley, Reading, MA, 1973.

2. Environmental Protection Agency Staff, "Proposed Emission Monitoring and Performance Testing Requirements: Stationary Sources." Federal Register, Vol. 39, No. 177, 11 Sep 1974.

3. Staff, "American Electric Power Annual Report 1974", pp. 23-29, 2 Broadway, NYC, NY 10004.

4. Cooney, J., "Proc. Symp. Electromagn. Sensing Earth Satellites", (R. Zirkind, ed.), pp. P1-P10, Polytechnic Press, Brooklyn, NY, 1965.

5. Leonard, D.A., "Observation of Raman Scattering from the Atmosphere Using a Pulsed Nitrogen UV Laser", Nature, 216, 142 (1967).

6. Inaba, H. and T. Kobayasi, "Laser-Raman Radar for Chemical Analysis of Polluted Air", Nature, 224, 170 (1969).

7. Kobayasi, T. and H. Inaba, "Spectroscopic Detection of SO_2 and CO_2 Molecules in Polluted Atmosphere by Laser-Raman Radar Technique", Appl. Phys. Letters, 17, 139 (1970).

8. Levatter, J., R. Sandstrom, and S. Lin, "Raman Cross Sections Measured by Short-Pulse Laser Scattering and Photon Counting", J. Appl. Phys., 44, 3273 (1973).

9. Fouche, D. and R.K. Chang, "Relative Raman Cross Sections for O_2, CH_4, C_3H_8, NO, N_2O, and H_2," Appl. Phys. Letters, 20, 256 (1972).

10. Schildkraut, E., "Pollution Analysis Using Remote Raman Spectroscopy", Amer. Laboratory, p. 23, Dec. 1972.

11. Kent, G. and R.W.H. Wright, "A Review of Laser Radar Measurements of Atmospheric Properties", J. Atmosph. Terr. Phys., 32, 917-943 (1970).

12. Kildal, H. and R.L. Byer, "Comparison of Laser Methods for the Remote Detection of Atmospheric Pollutants", Proc. IEEE 59, 1644-1663 (1971).

13. Inaba, H. and T. Kobayasi, "Laser-Raman Radar", Optoelectronics, 4, 101-123 (1972).

14. Nakahara, S., et al., "Detection of Sulphur Dioxide in Stack Plume by Laser Raman Radar", Optoelectronics, 4, 169-177 (1972).

15. Darling, R., 2006 Karen Lane, Tallahassee, FL 32304.

16. Melfi, S.H., M.L. Brumfield, and R.W. Storey, "Observation of Raman Scattering by SO_2 in a Generating Plant Stack Plume", Appl. Phys. Letters, 22, 402 (1973).

17. Northam, G.B. and M.L. Brumfield, private communication, 1973.

18. Nakahara, S., K. Ito, and S. Ito, private communication, 1972.

19. Gelbwachs, J. and M. Birnbaum, "Fluoresence of Atmospheric Aerosols and Lidar Implications", Appl. Optics, 12, 2442 (1973).

20. Leonard, D., "Measurement of Aircraft Turbine Engine Emissions", in Laser Raman Gas Diagnostics (M. Lapp and C. Penney, eds.), pp. 45-61, Plenum Press, NY (1974).

21. Hirschfeld, T., et al., "Remote Spectroscopic Analysis of PPM-Level Air Pollutants by Raman Spectroscopy", Appl. Phys. Letters, 22, 38-40 (1973)

22. DeLong, H.P., "Air Pollution Field Studies with a Raman Lidar", Optical Engineering, 13, 5 (1974).

23. Melfi, S.H., "Remote Raman Scattering Probes", in Laser Raman Gas Diagnostics (M. Lapp and C. Penney, eds.), pp. 231-247, Plenum Press, NY (1974).

24. Kuper, G., private communication, 1975.

25. Blifford, I., "Factors Affecting the Performance of Commercial Interference Filters", Appl. Optics, 5, 105 (1966).

26. Brynn, S., private communications, Ditric Optics, 1974.

27. Schofield, K., "Molecular Fluorescence as a Monitor of Minor Stratospheric Constituents", NASA CR-2513, NASA Washington, DC, Feb. 1975.

28. Eggeman, R.T., Eppley Laboratory, Inc., 1973.

29. Ramsey, W.Y., "Specular Spectral Reflectance of Paints from 0.4 to 40.0 Microns", Report 31, Meteorological Satellite Laboratory, Washington, DC (1964).

30. Leonard, D. and B. Caputo, "A Single-Ended Atmospheric Transmissometer", Optical Engineering, 13, 1, p. 10 (1974).

31. Cook. G., G. Be hke, and W. Conner, "Remote Measurement of Smoke Plume Transmittance Using Lidar", Appl. Optics, 11, 1742 (1972).

32. Conner, W., "Measurement of the Opacity and Mass Concentration of Particulate Emissions by Transmissometry", EPA-650/2-74-128, Research Triangle Park, NC (1974) (see also EPA-650/2-74-120).

33. Collis, R.T.H. and E.E. Uthe, "Mie Scattering Techniques for Air Pollution Measurement with Lasers", Optoelectronics, 4, 87-99 (1972).

34. Johnson, W. and E. Uthe, "Lidar Study of the Keystone Stack Plume", Atmosph. Environment, 5, 703-724 (1971).

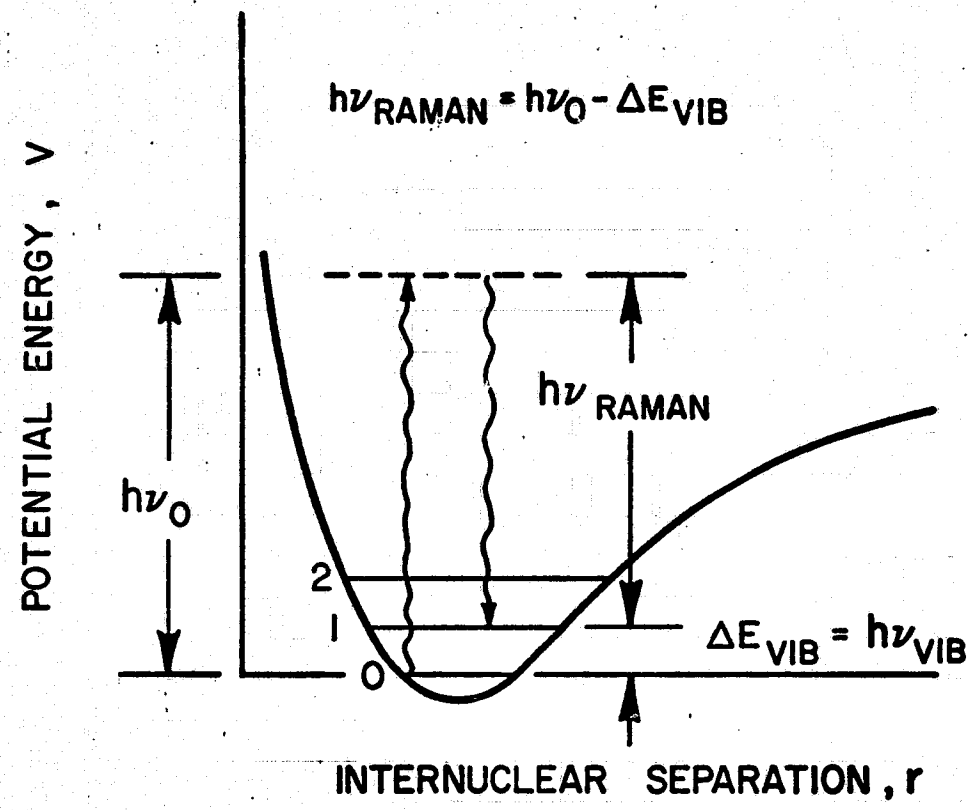

Figure 1. Vibrational Raman Scattering (after Leonard, 1972).

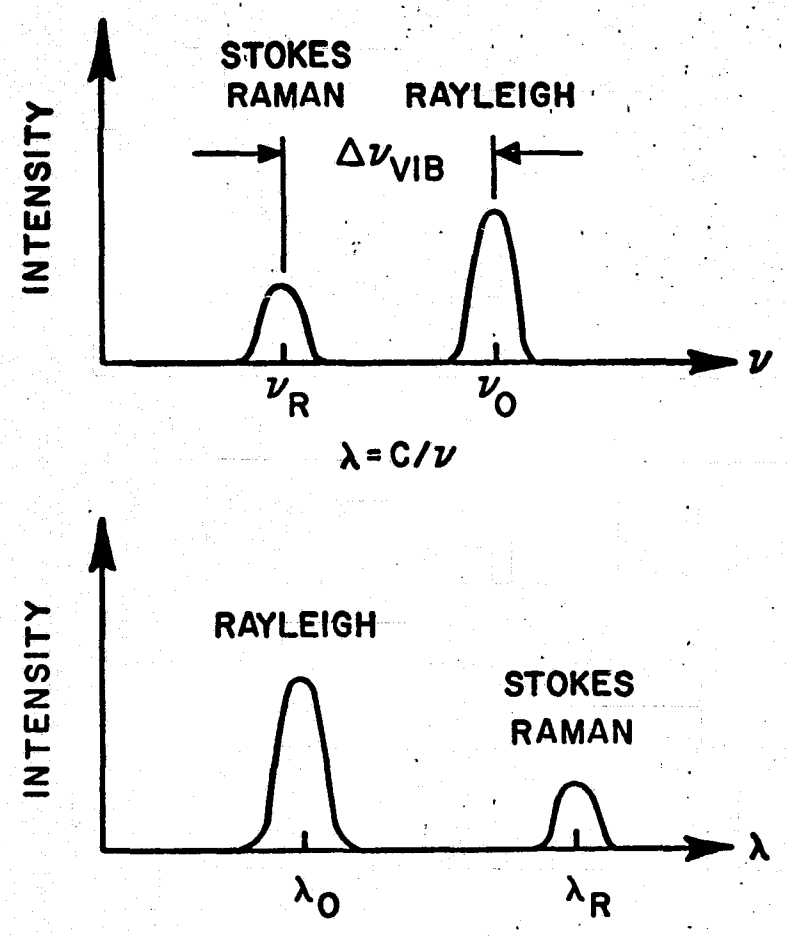

Figure 2. Raman Shifts in Frequency and Wavelength.

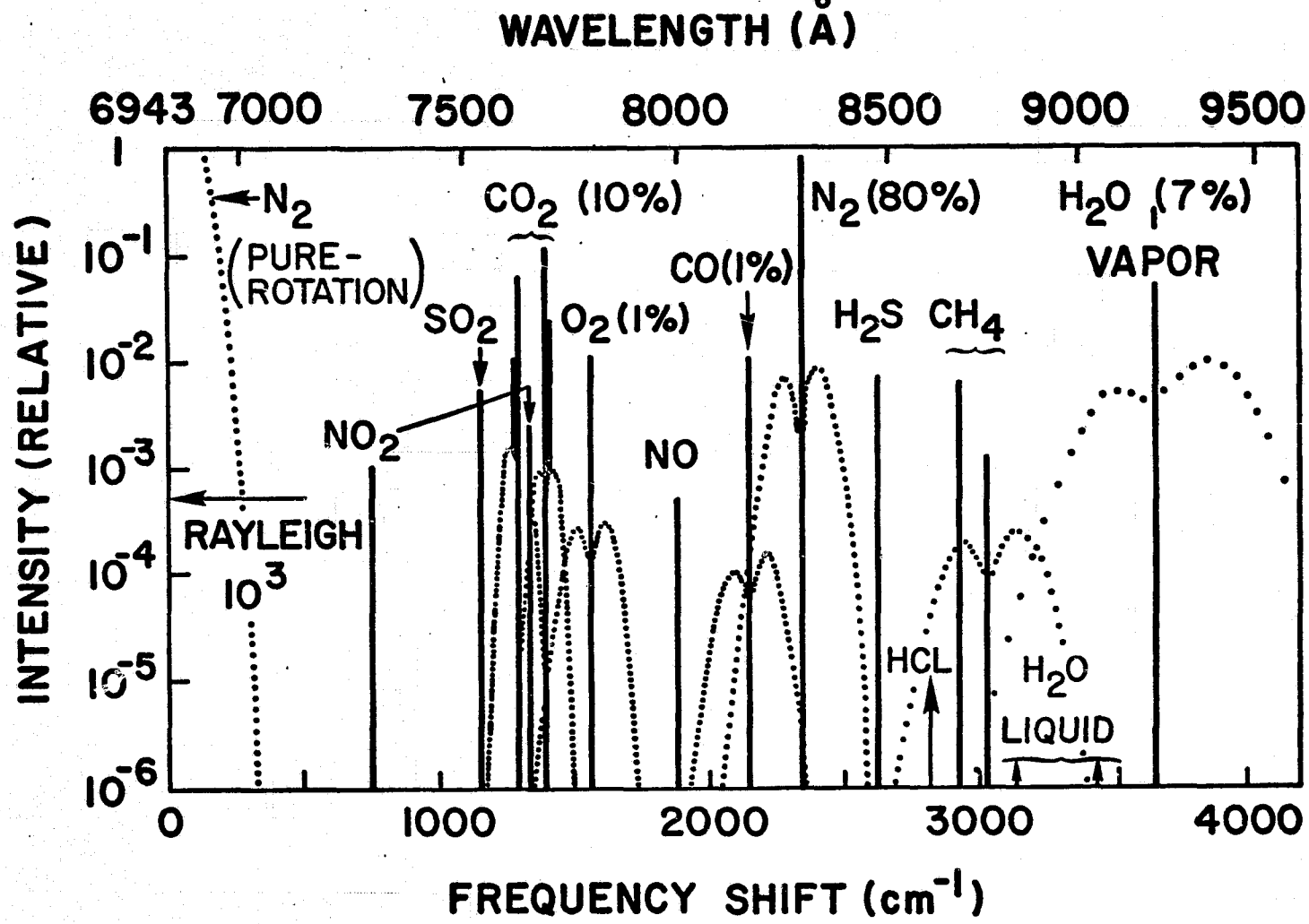

Figure 3. Raman Backscatter Function (Theoretical) for Typical Oil Smoke Plume Using Ruby Lidar (after Inaba and Kobayasi, 1972). SO_2 Concentration is 1000 ppm. Positions of Scatter from HCl and Liquid Water are Also Indicated.

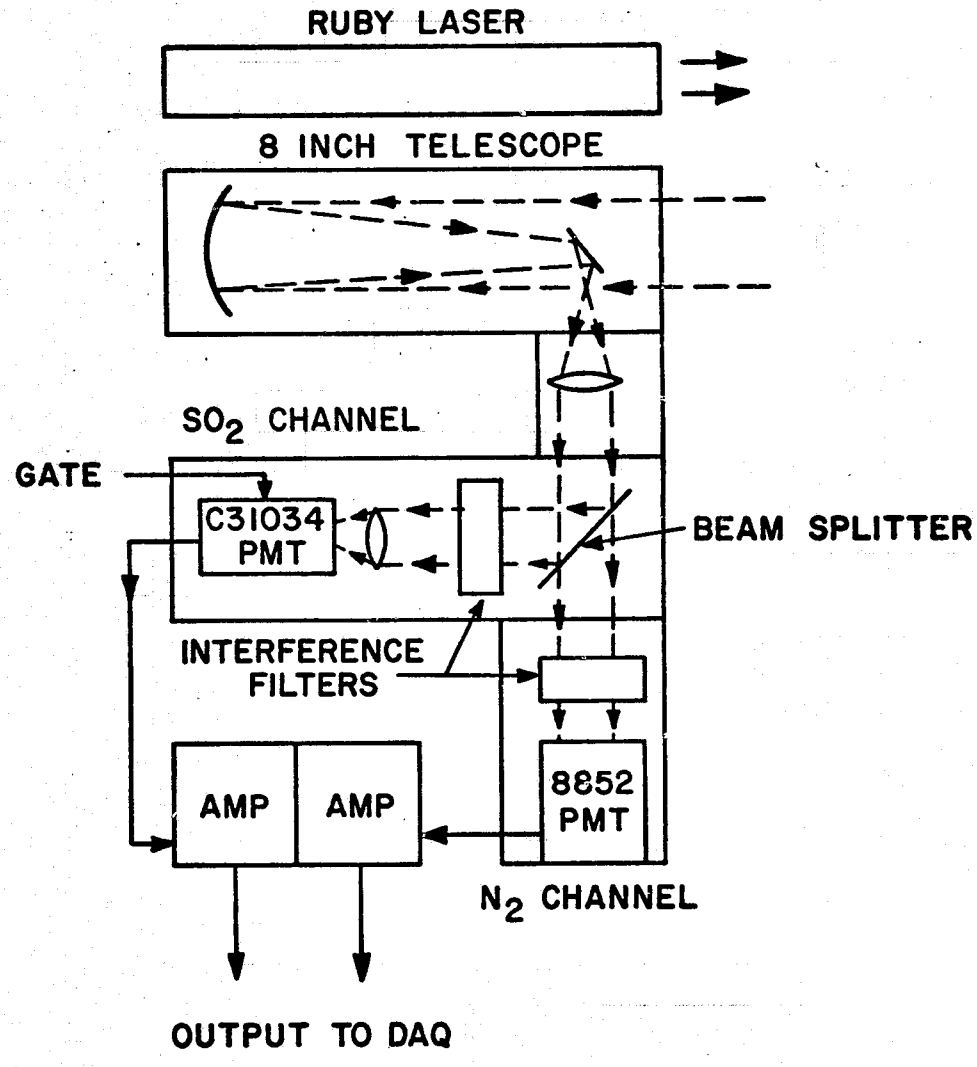

Figure 4. Laser and Receiver of NASA-Langley Raman Lidar.

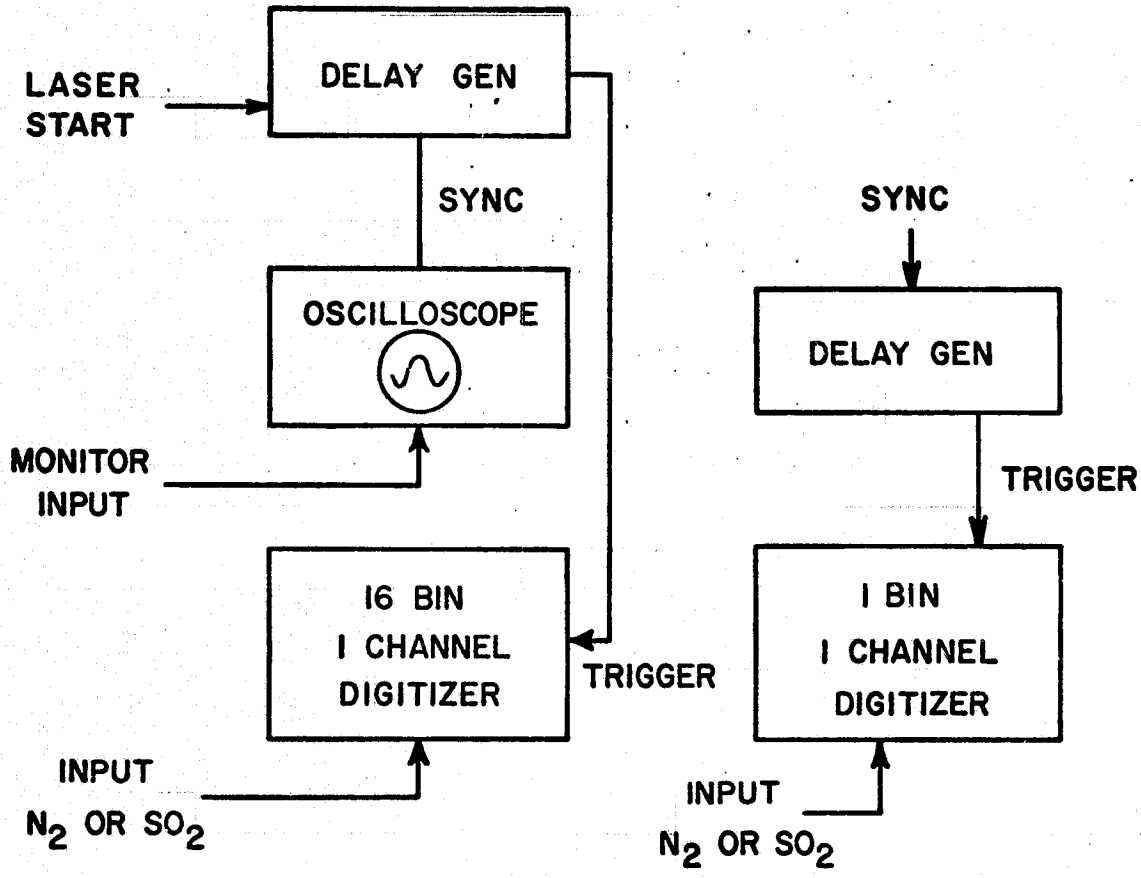

Figure 5. Data Acquisition System of NASA-Langley Lidar.

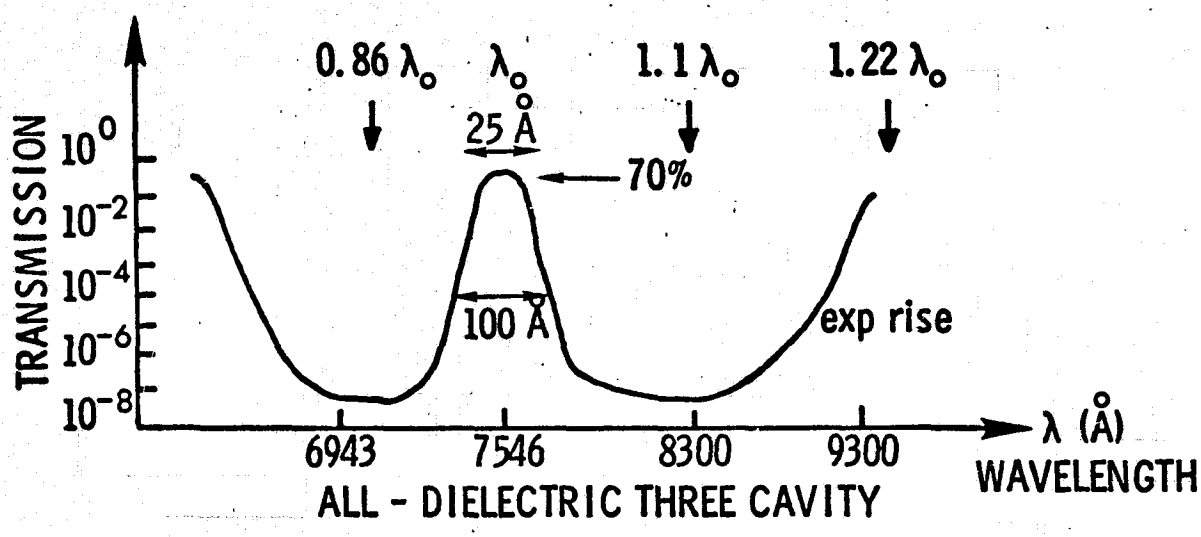

Figure 6. Typical Performance of All-Dielectric Interference Filters.

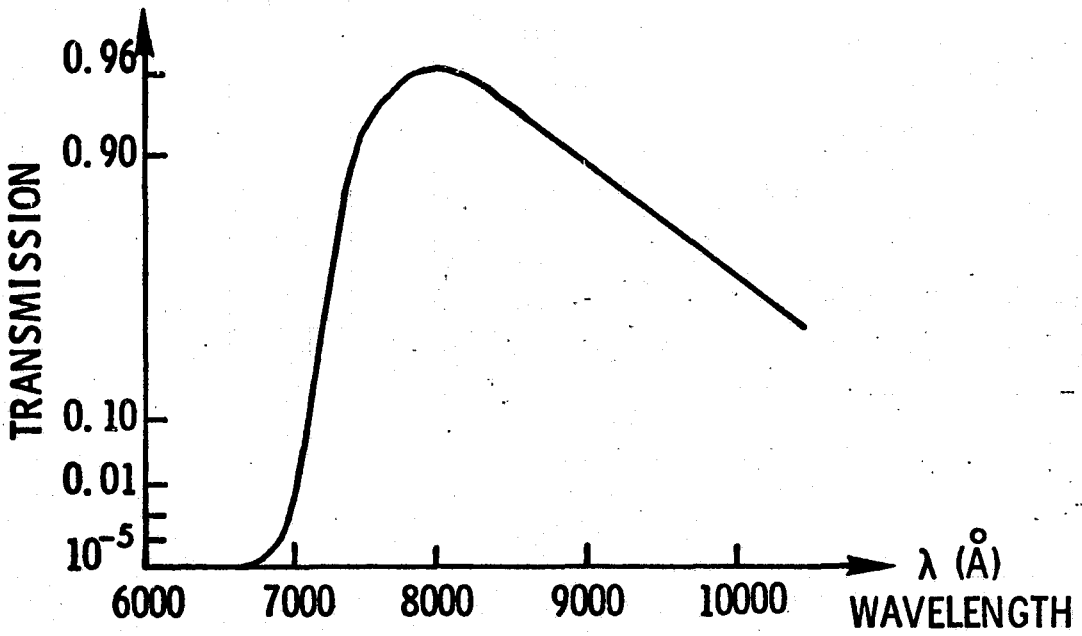

Figure 7. Tranmission of 3-mm Thickness RGN-9 Schott Glass Absorber.

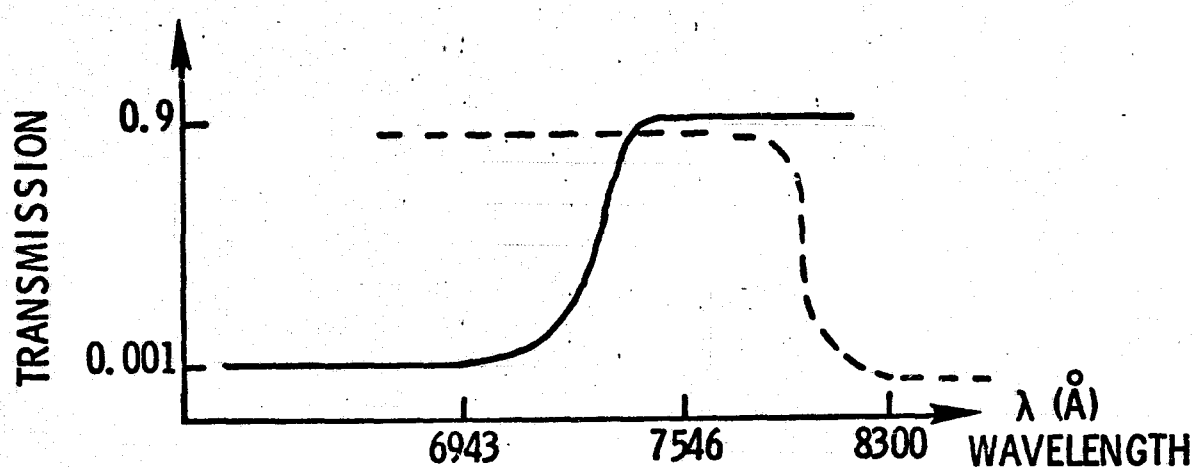

Figure 8. Optimum Beamsplitters for Raman Scatter Separation.

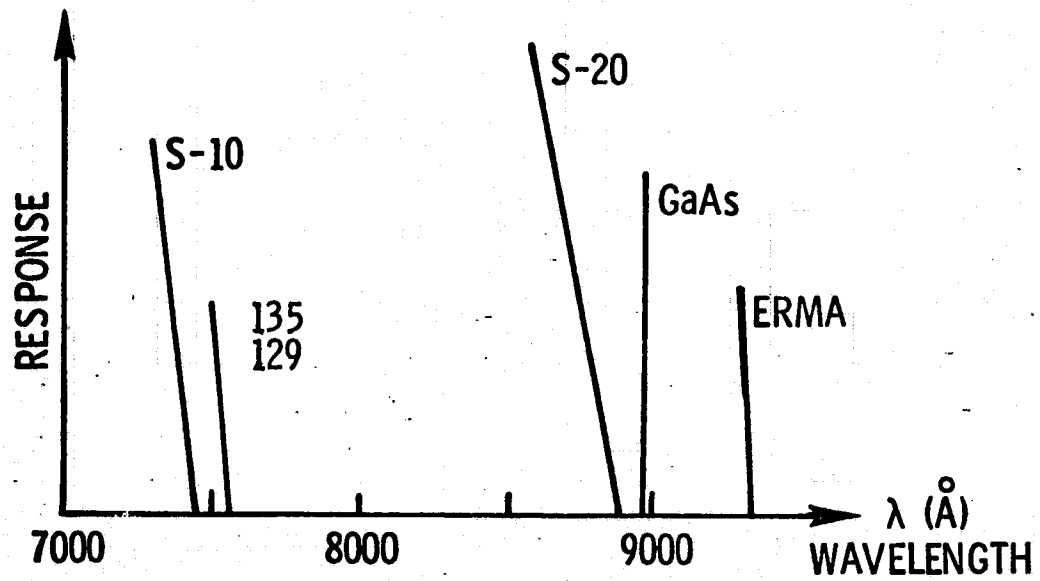

Figure 9. Wavelengths of Response Cut-offs of Several Photomultipliers.

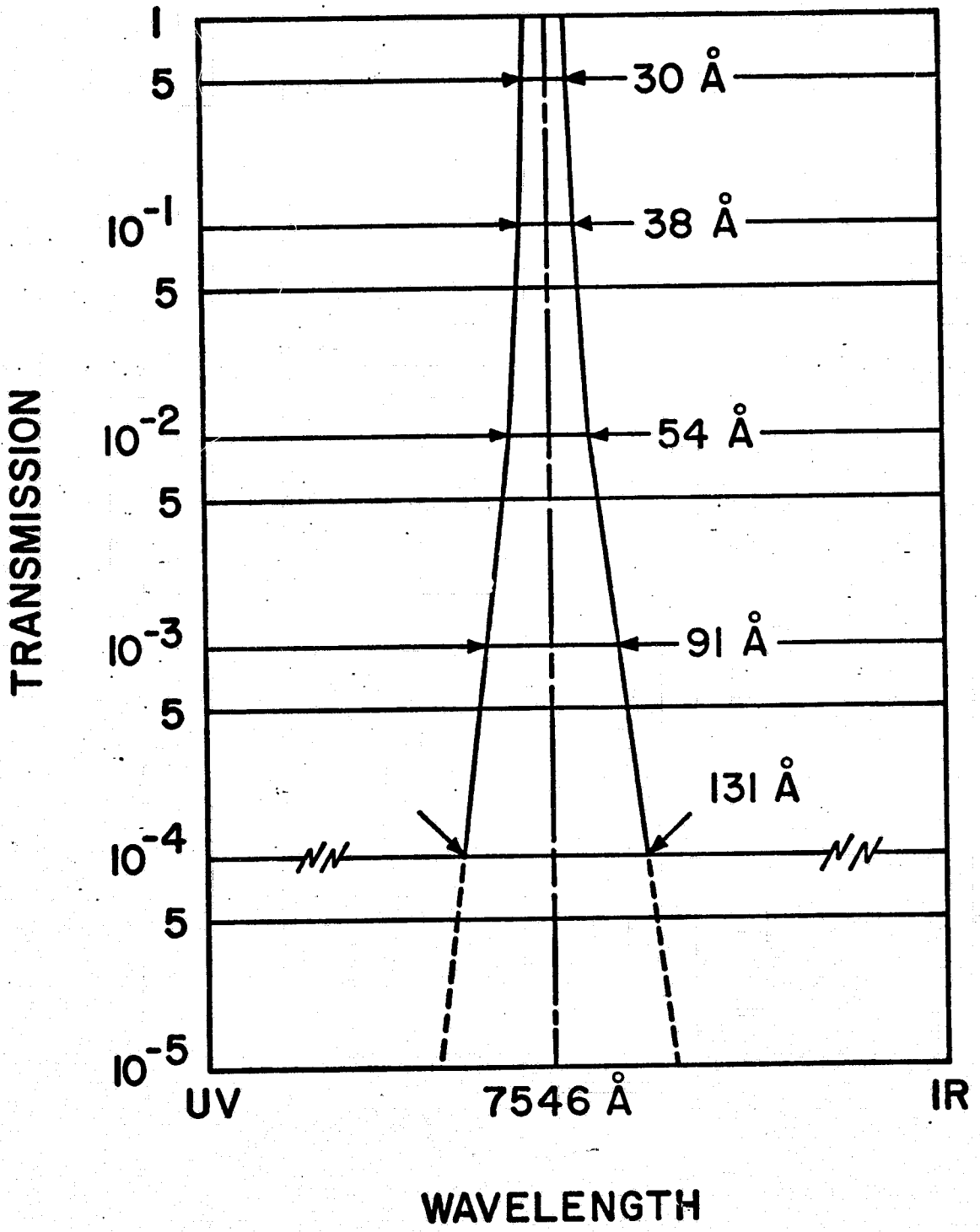

Figure 10. Typical Behavior of Three-Period Interference Filter with 30 Å Full Width at Half Maximum. (Ditric Optics).

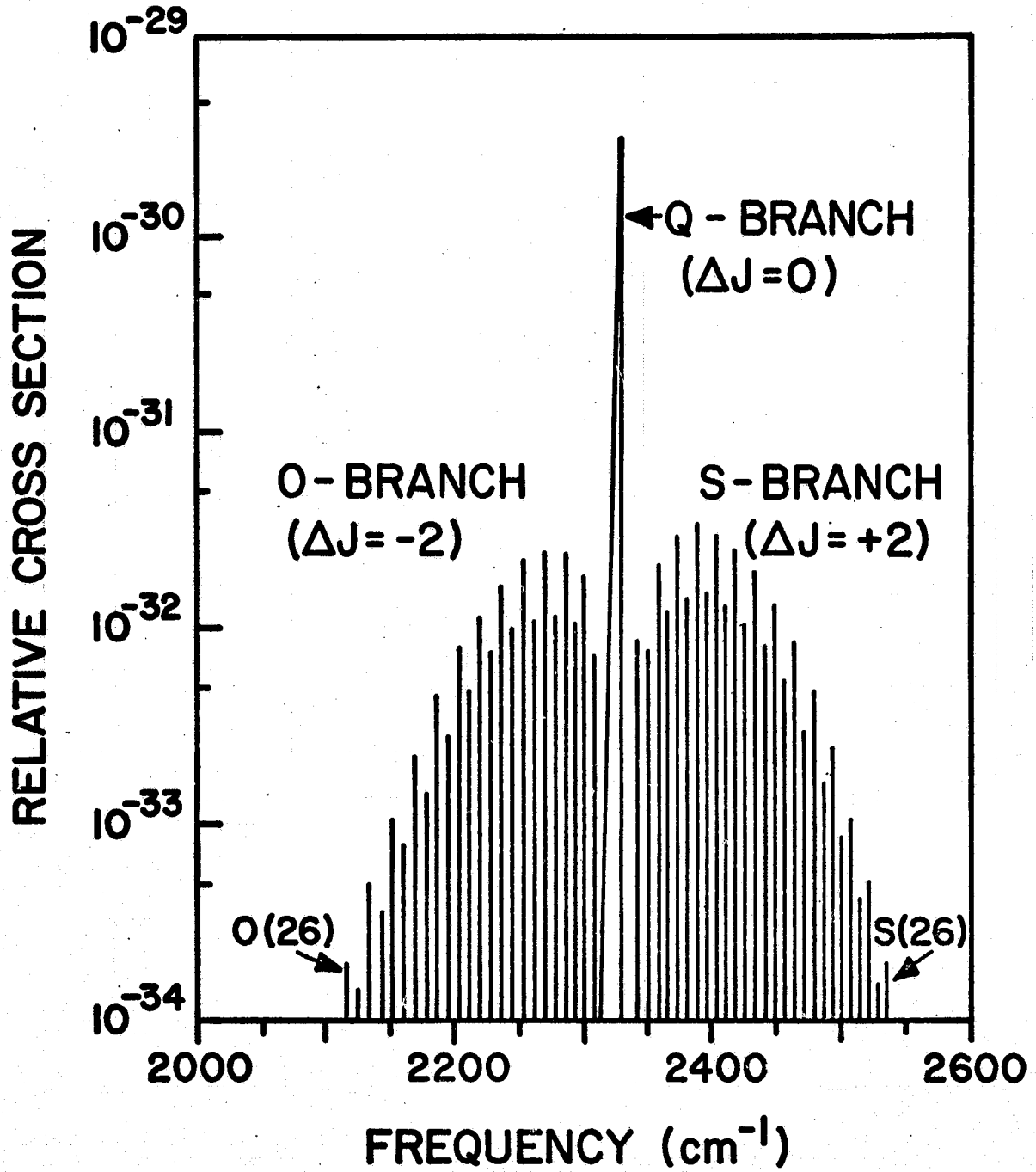

Figure 11. Rotational Structure of Nitrogen Raman Scatter ($\nu = 0 \rightarrow 1$) at 300° K (after Inaba and Kobayasi, 1972).

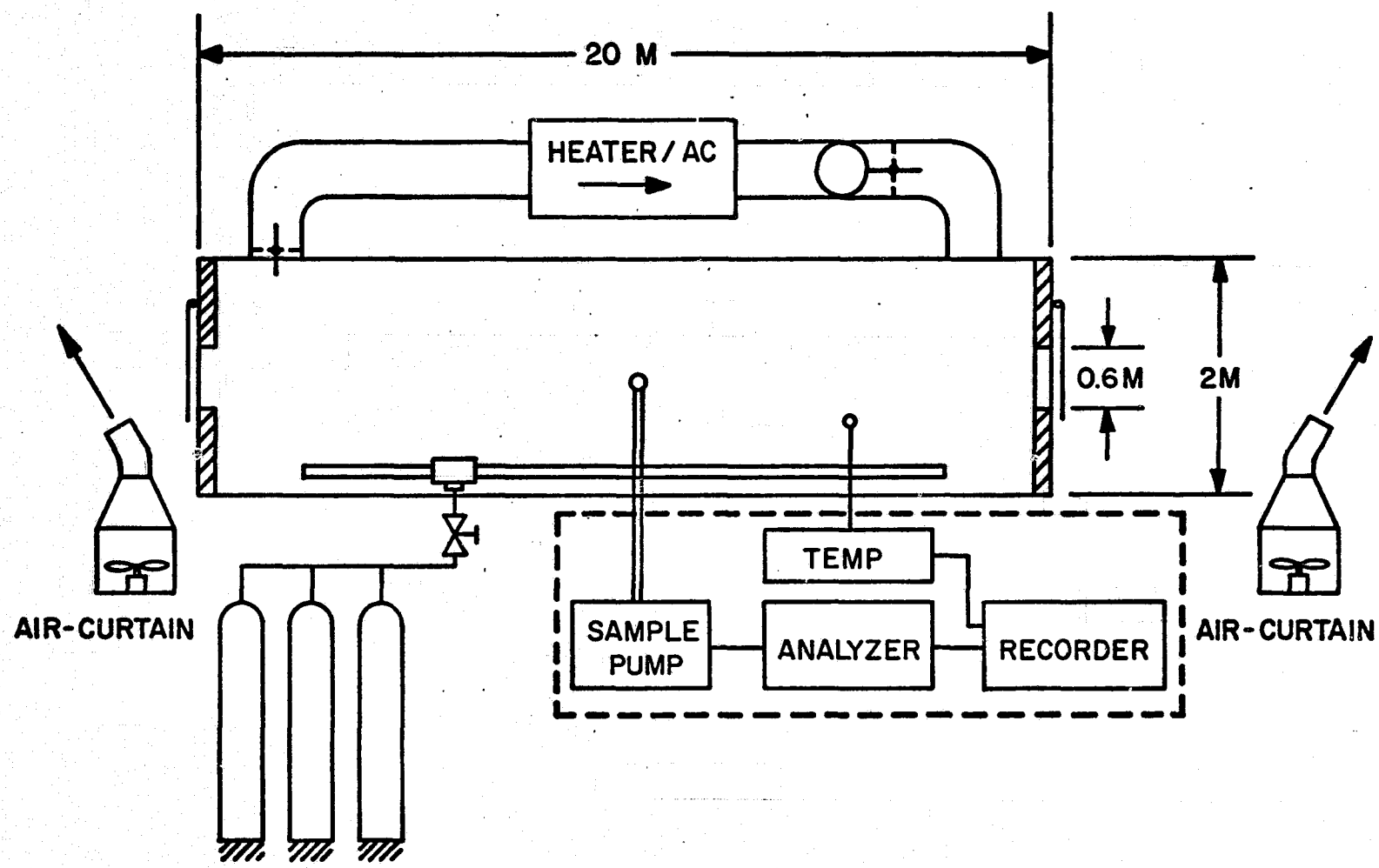

Figure 12. Calibration Tank Schematic.

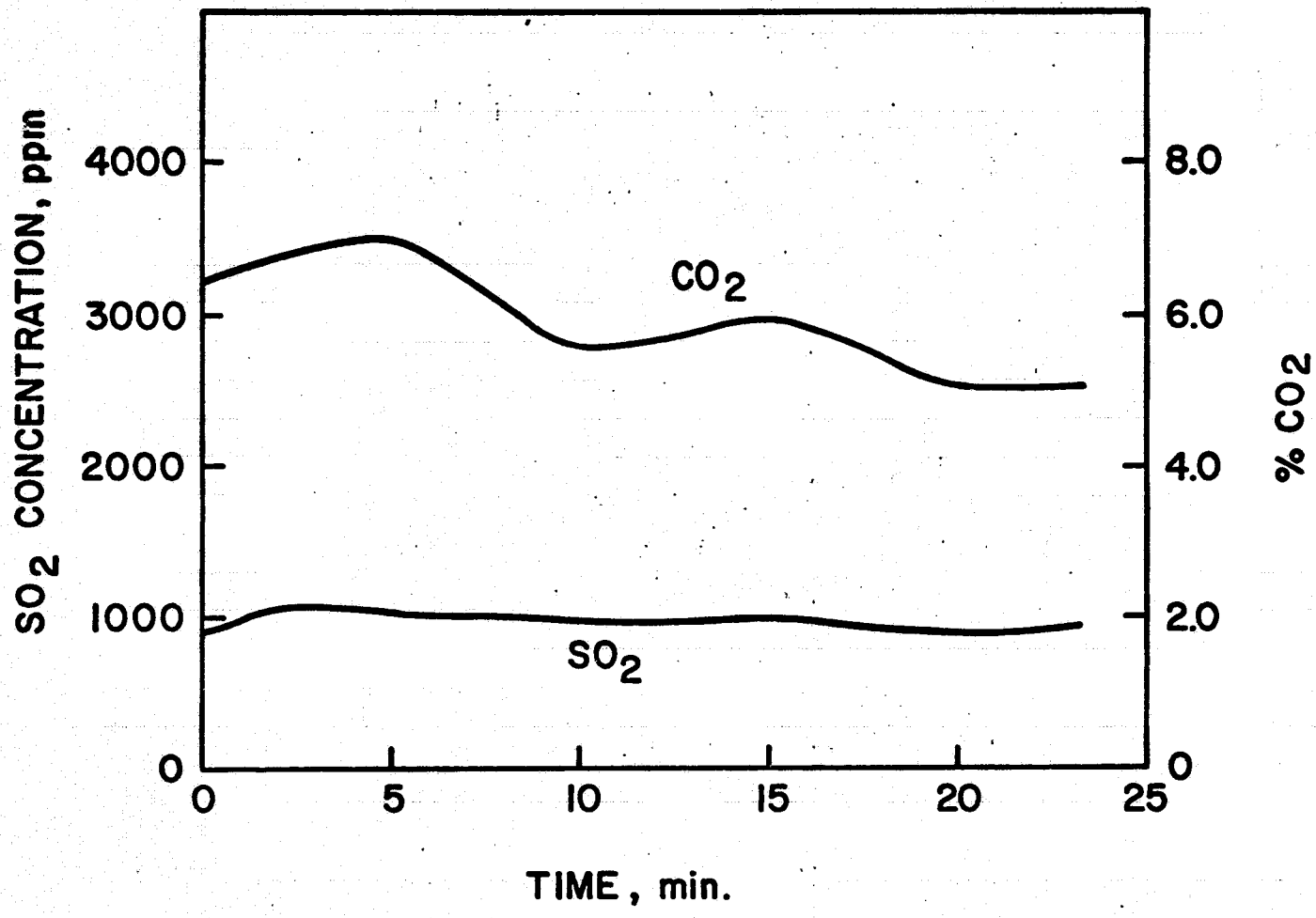

Figure 13. Calibration Tank Performance for Several Gases.

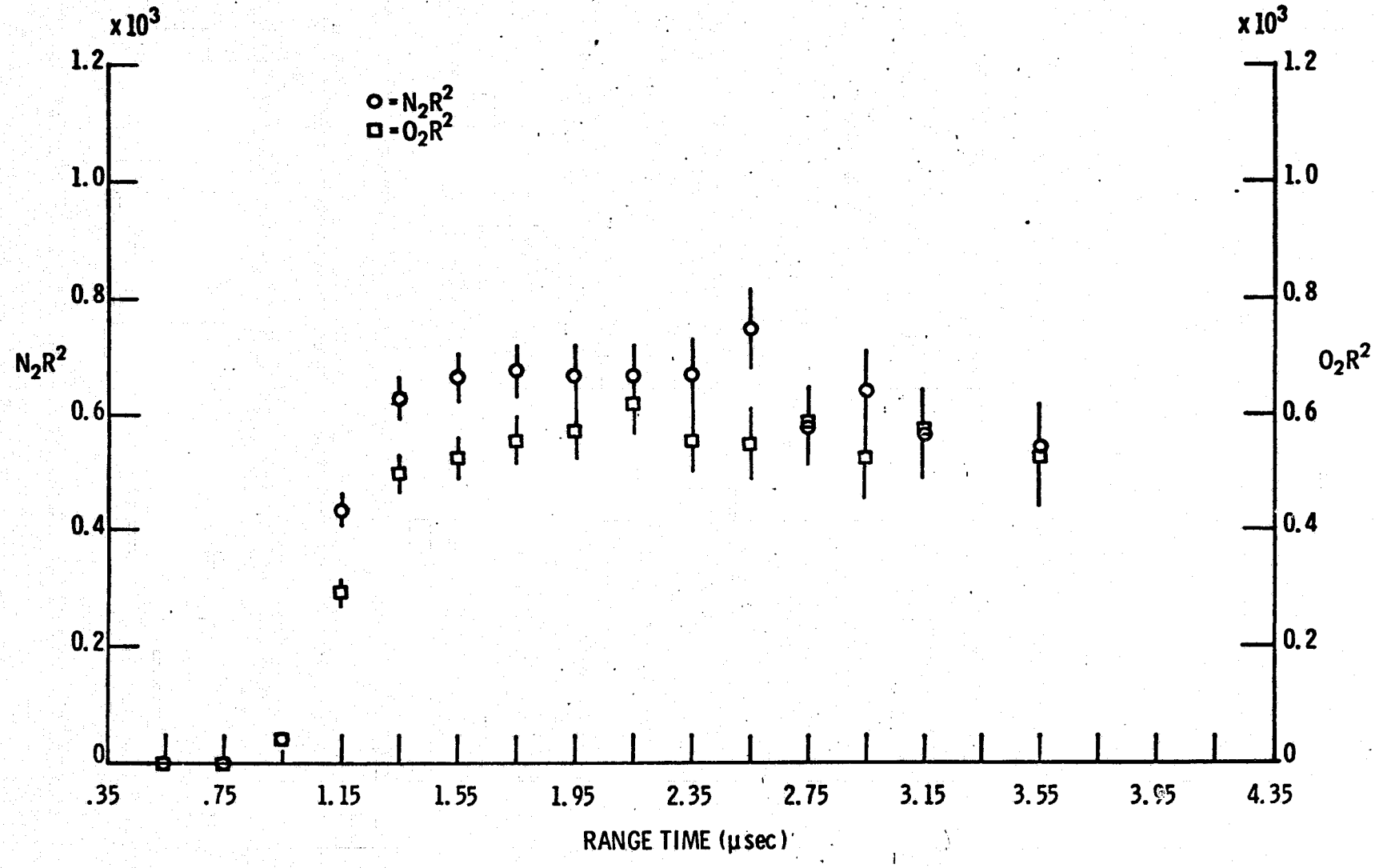

Figure 14. Raman Signal from N_2 and O_2 in the Atmosphere.

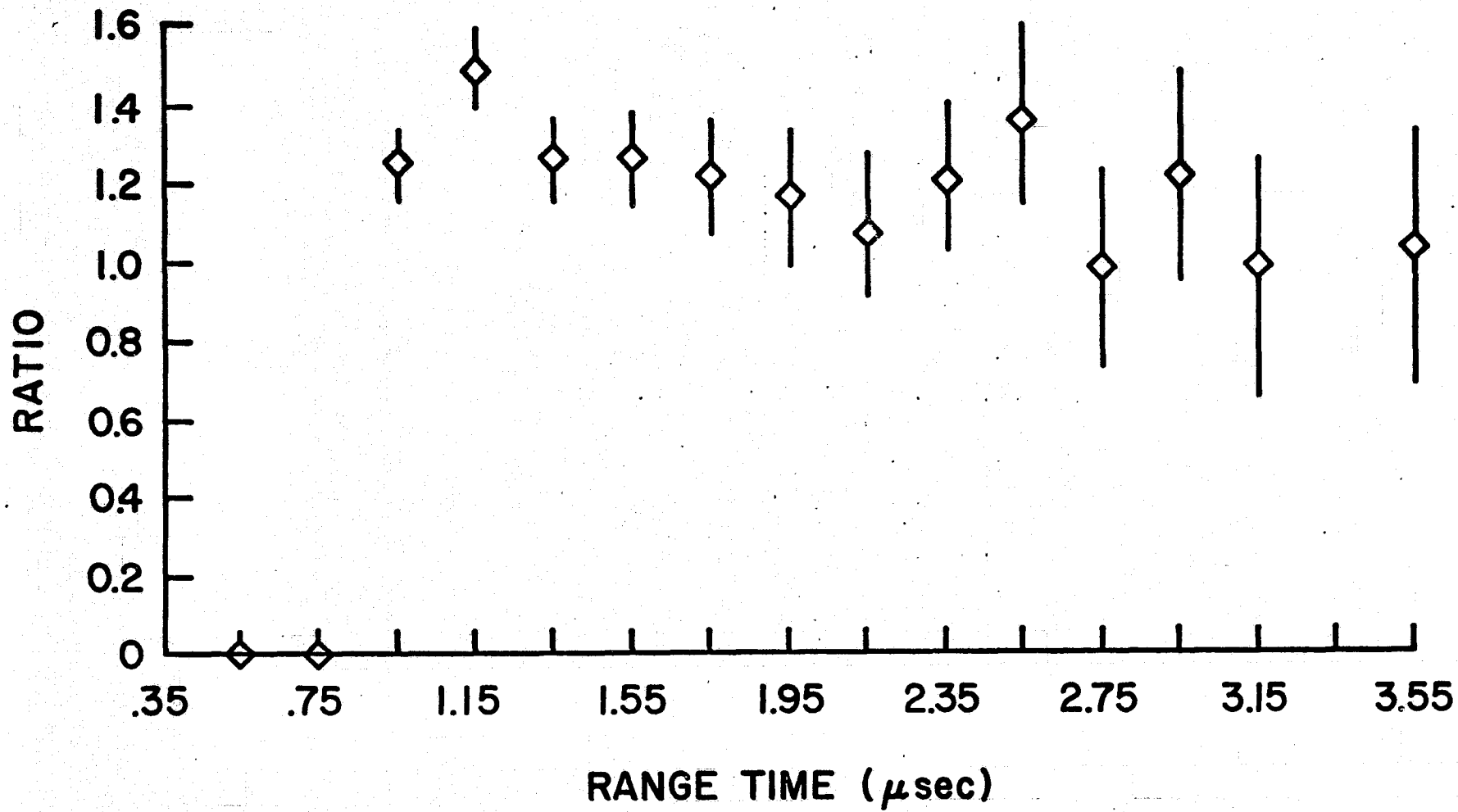

Figure 15. Ratio of the Range Corrected N_2 and O_2 Profiles in the Atmosphere.

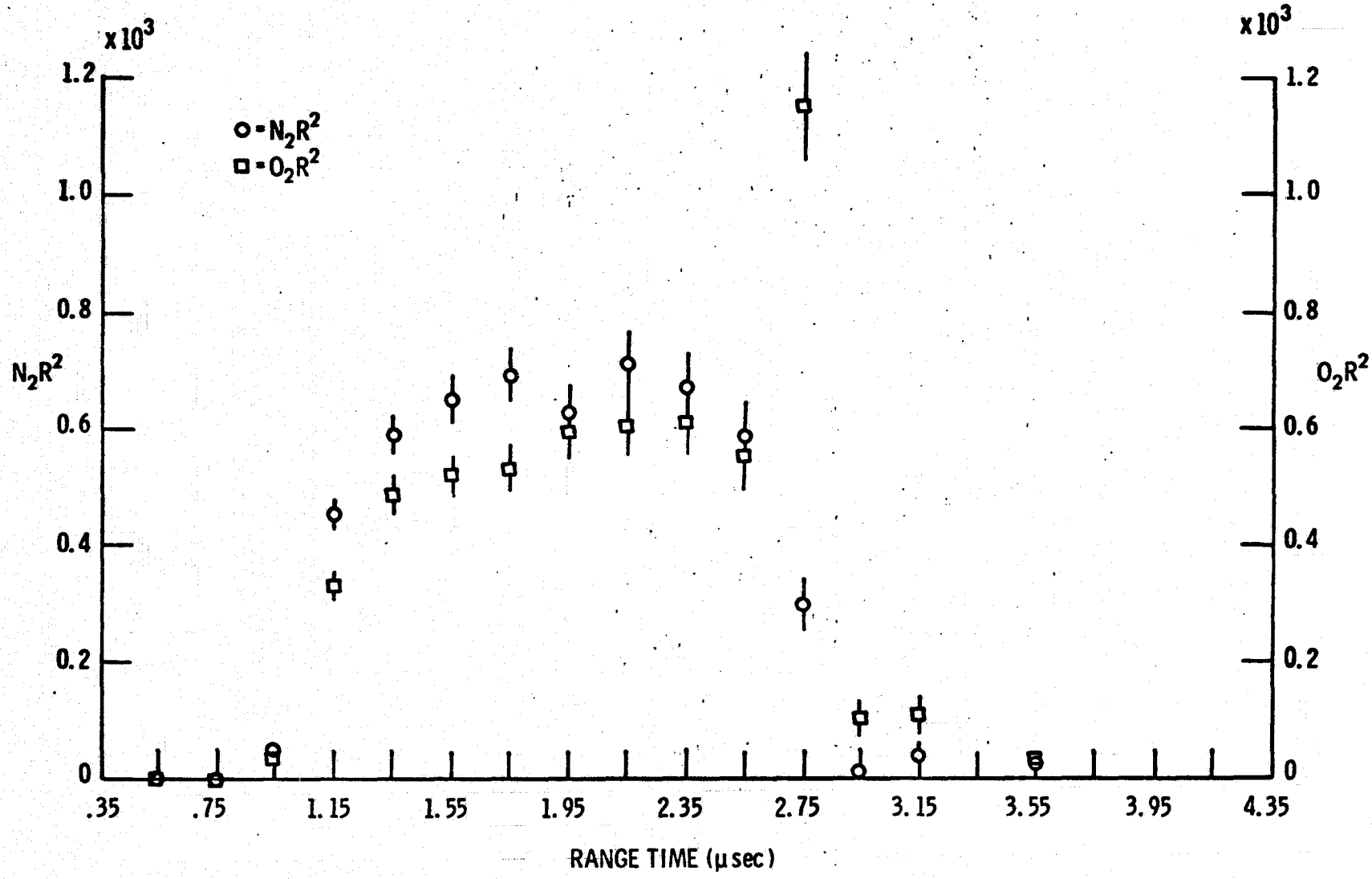

Figure 16. Raman Signal from N_2 and O_2 Through the Calibration Tank with 200 nsec Bins.

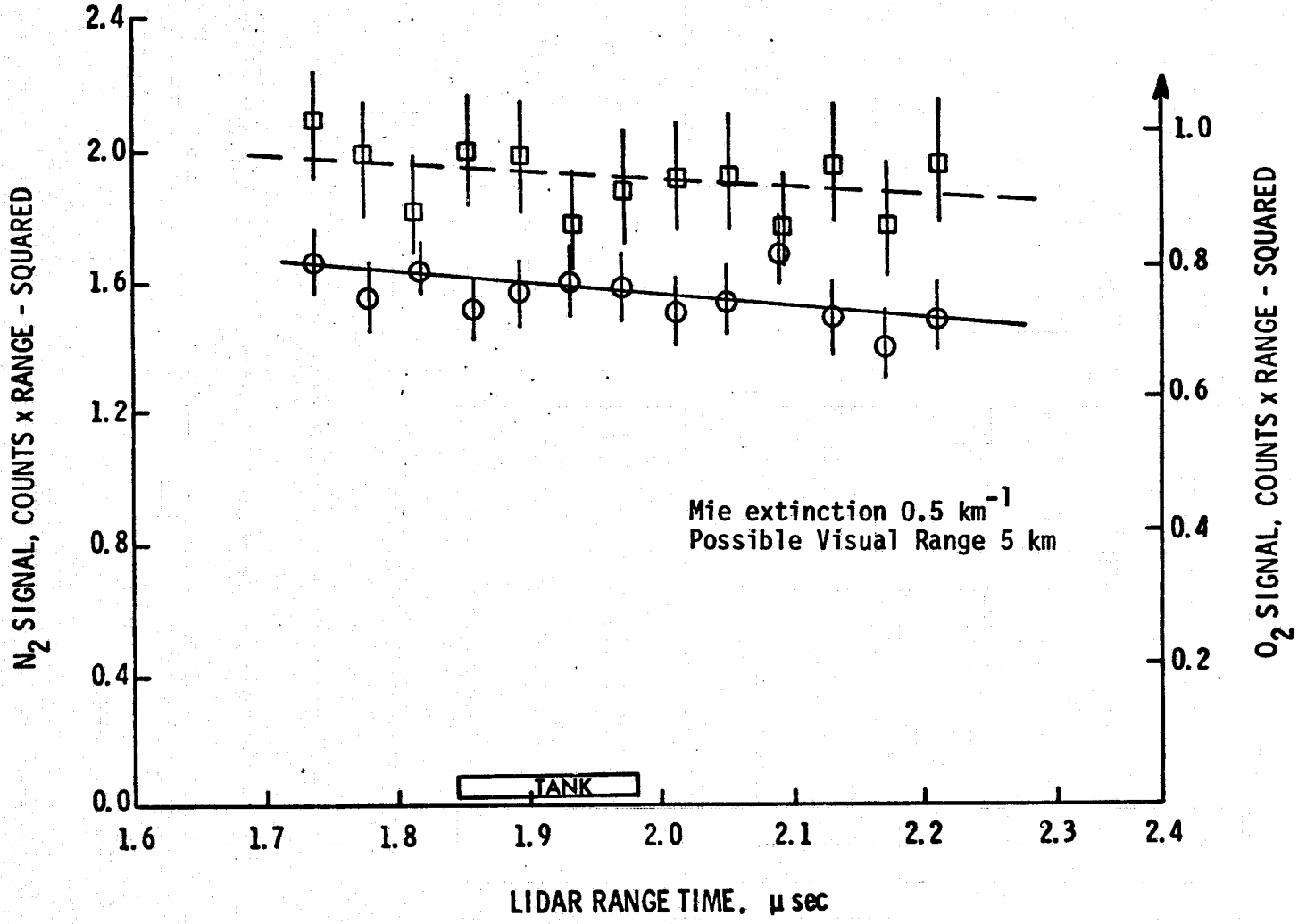

Figure 17. Raman Signal from N_2 and O_2 Through the Calibration Tank with 40 nsec Bins.

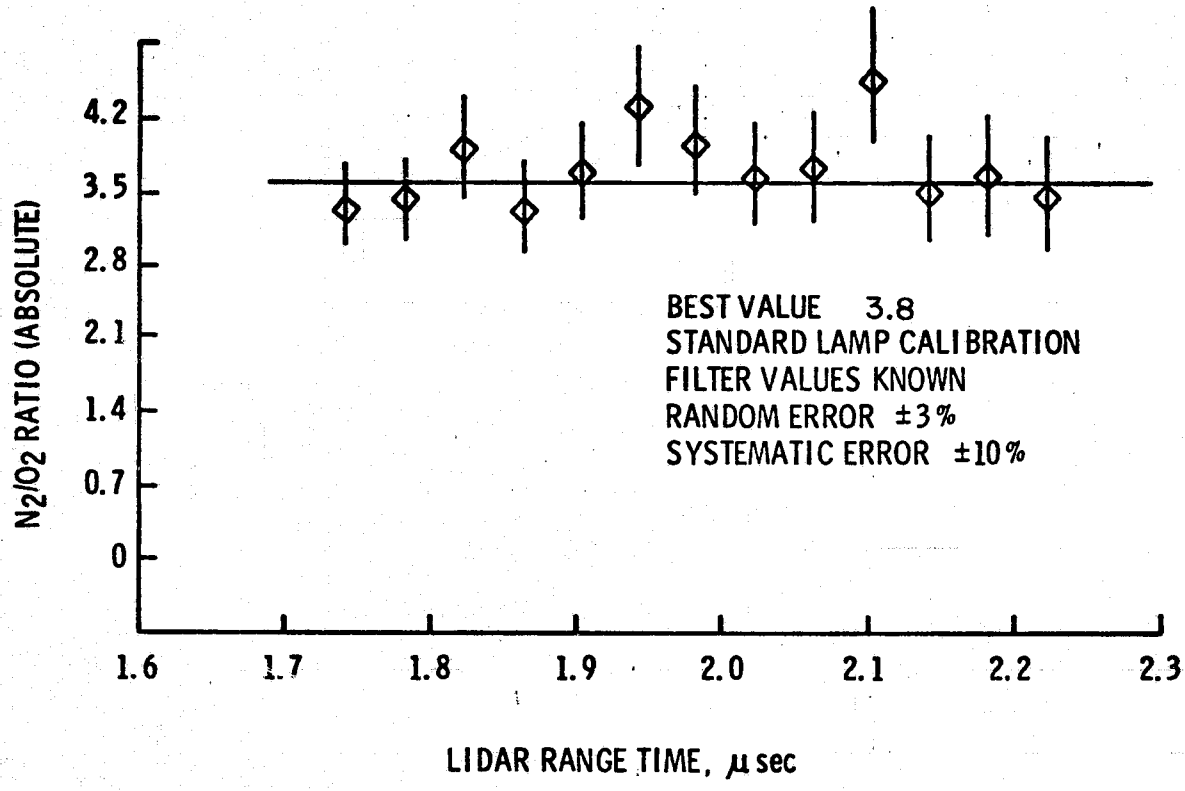

Figure 18. Ratio of the Range Corrected N_2 and O_2 Profiles Through the Calibration Tank.

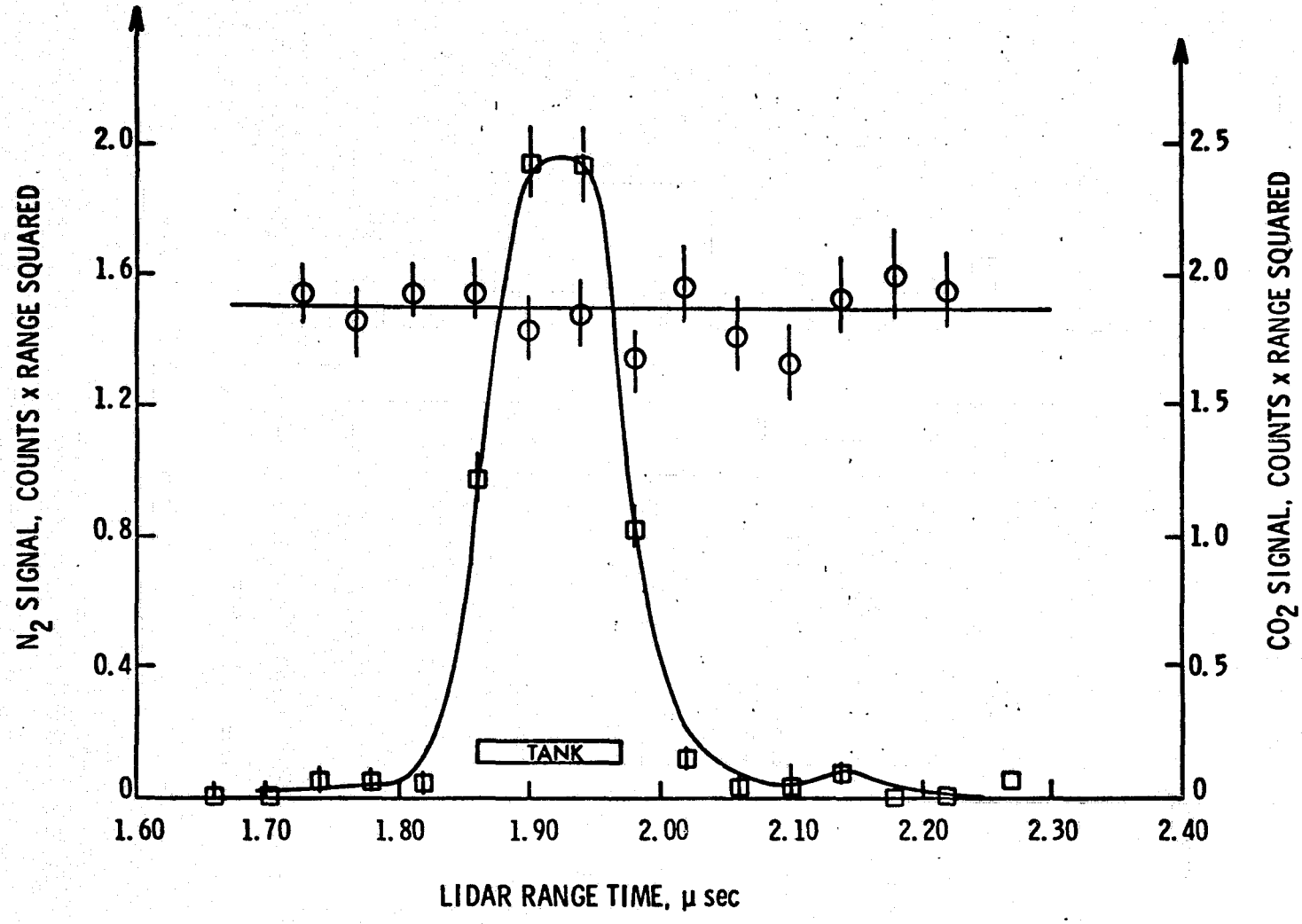

Figure 19. Raman Signal from High Concentration CO_2 in the Calibration Tank. Nitrogen Reference Signal is Included.

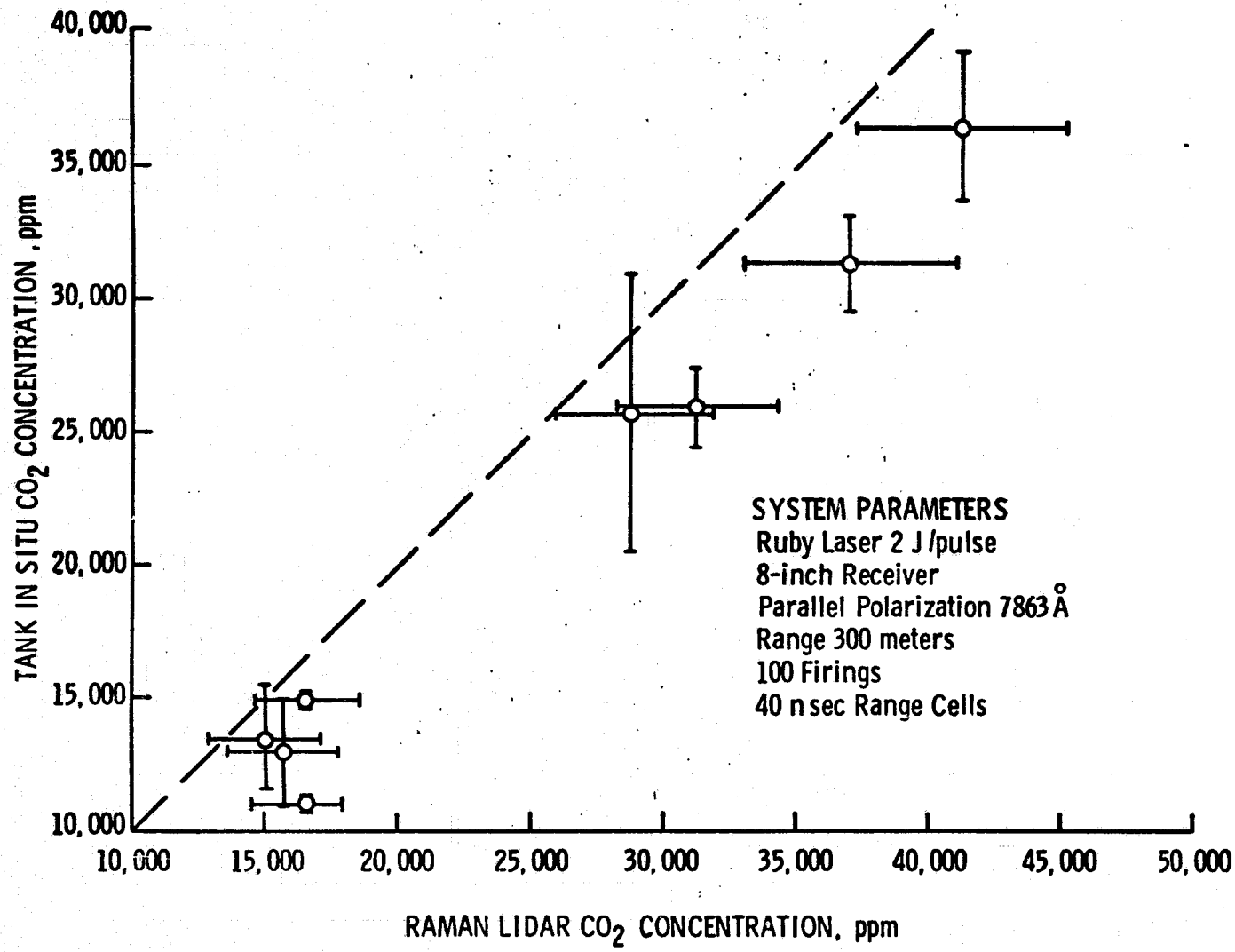

Figure 20. Comparison of CO_2 Raman Lidar Measurements with In Situ Gas Analysis.

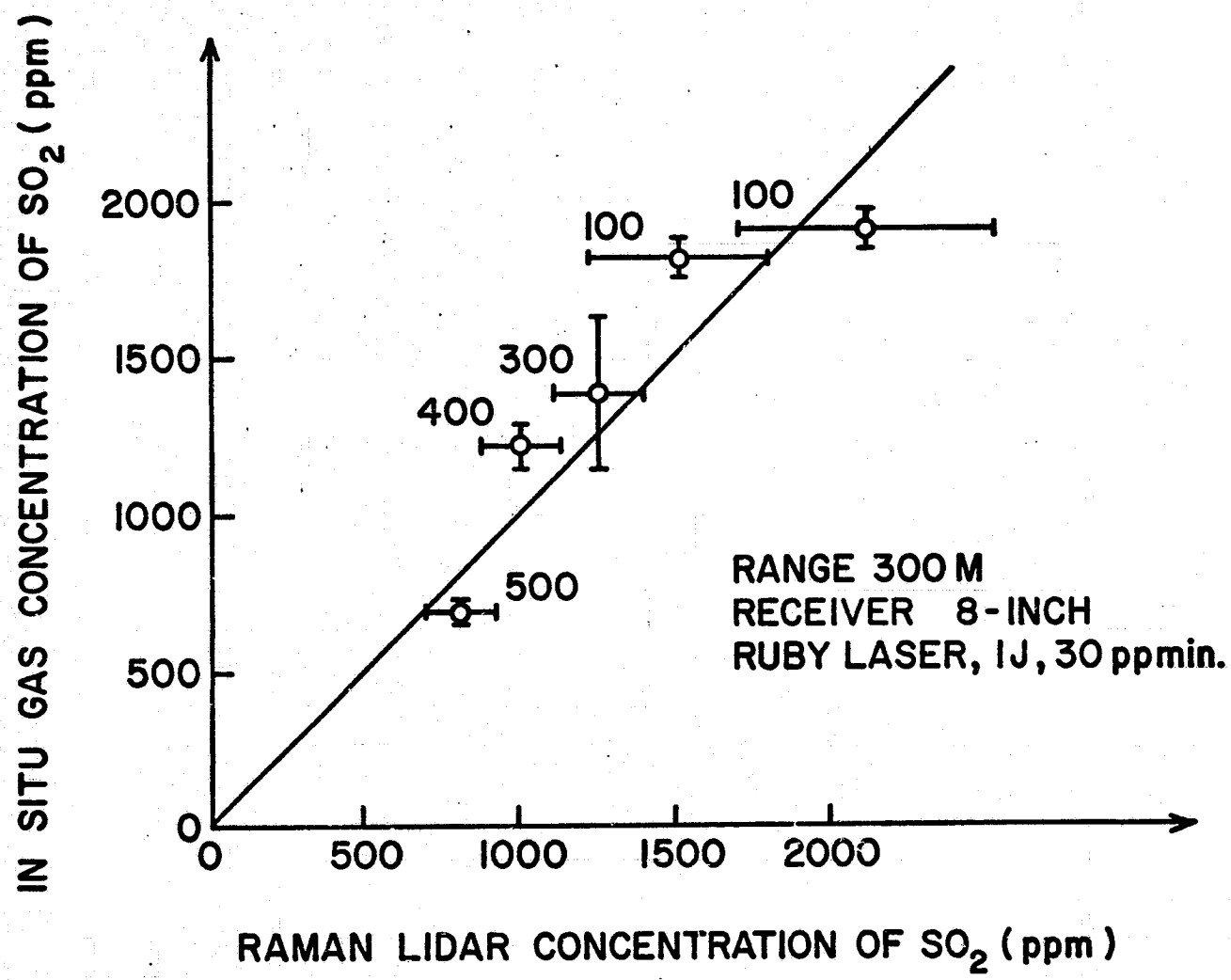

Figure 21. Comparison of SO_2 Raman Lidar Measurements with In Situ Gas Analysis.

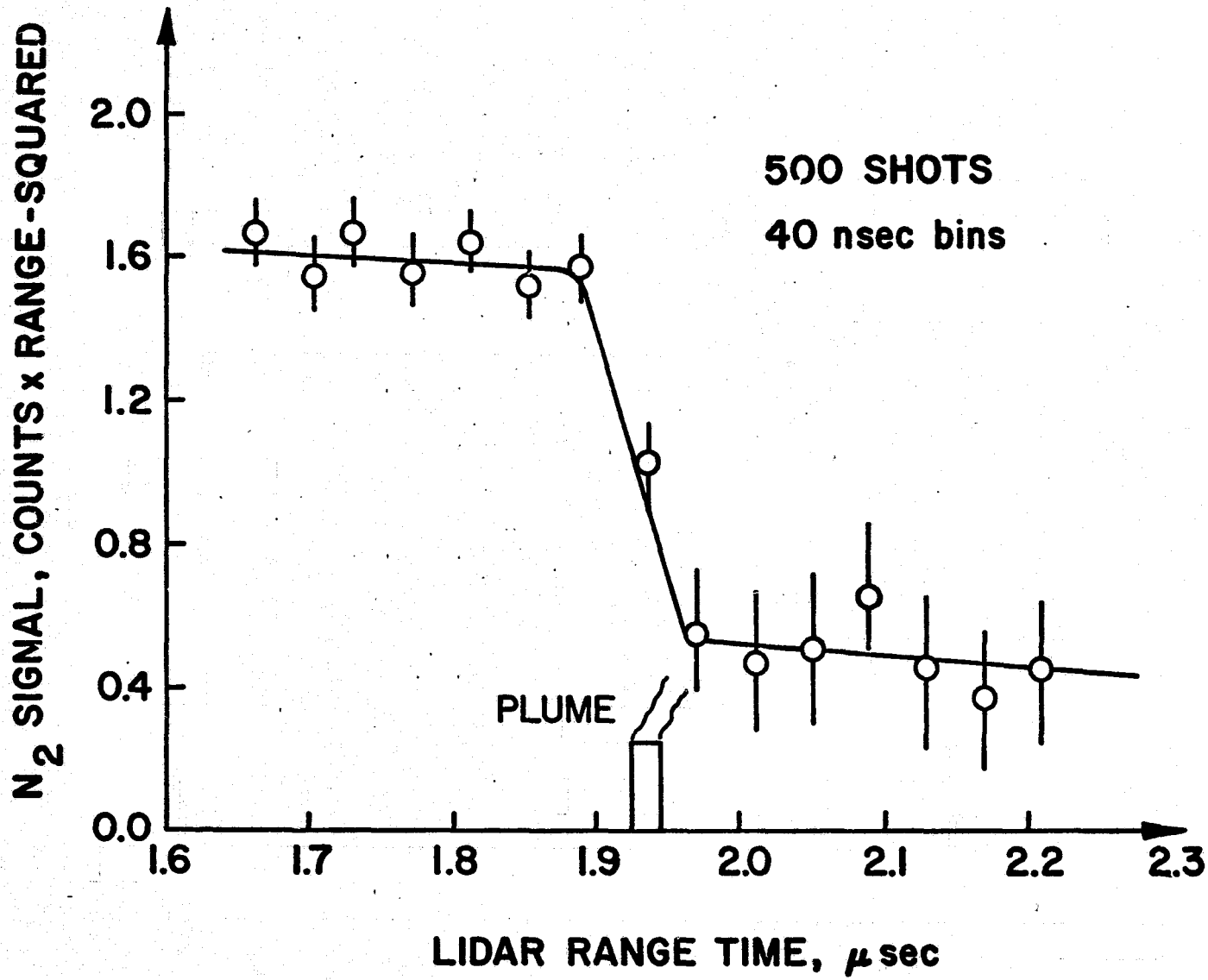

Figure 22. Schematic of Nitrogen Raman Return Expected When Viewing Through a Stack Plume.

APPENDIX 1

DATA ACQUISITION OPTIONS AND DATA ANALYSIS PROGRAMS

C.F. Jones, LTV Corp., Hampton, VA 23665

and

S.K. Poultney, Old Dominion University

MEMORANDUM

SUBJECT: Raman LIDAR Data Reduction Program DATE: 1 August 1975

TO: Dr. G. B. Northam, NASA/ESSD FILE: V-19000/5NAS- 208

FROM: Ms. C. F. Jones, LTV/HTC

CC: Mr. M. L. Brumfield, NASA/ESSD
Mr. T. E. Chappell, LTV/HTC
Dr. S. Poultney, ODU

I. INTRODUCTION

Data from the Raman LIDAR project can be taken in single or dual channel modes. Two classes of LIDAR operations occur: a pulsed-laser class which is used to monitor Raman backscatter from one or more types of gases; and a standard lamp class which is used to calibrate the LIDAR. The data reduction program was designed to be able to handle any combination of these modes and classes by keying on several input parameters. In the single channel mode, there are numbers in 16 bins corresponding to data return as a function of time. If a single mode is used, that mode is usually repeated for and paired with another possible channel of operation. The numbers in each bin are usually the result of an accumulation of counts over a certain time period of operation (here measured in laser firings). The program will average compatible sets of such operation for up to two gas types and adjust for the range-squared dependence in the LIDAR equation for the laser-pulsed class of operation. Error bars are calculated for each point. The resulting data is fit with an exponential whose exponent is a measure of atmospheric extinction in the case of laser operation on an atmospheric constituent and then plotted. With paired single channel modes or with dual channel modes, this data is then ratioed, plotted on a separate graph with error bars, and fit with a horizontal line. All standard lamp measurements must be analyzed omitting the range-squared correction, of course. In the dual mode, the 16 bin single channel is split into two interleaved parts; with different gas types or standard lamp wavelengths recorded at the same laser firing. The program proceeds as above for each of the interleaved parts except that points for the ratio must be picked off from the best fit exponentials prior to ratioing.

II. INPUT

The first data card feeds general information to the program. An example appears in Appendix I. The input constants are as follows:

BT - Initial time delay (usec) between laser firing and data acquisition.

TAU - Time width (usec) of successive bins

F - A pile-up correction factor

TYPE1 and TYPE2 - Types of gas to be analyzed

IDUAL - Code = 1 for single channel mode; = 2 for dual channel.

ISTL - Code = 1 for laser firing mode; = 1 for standard lamp mode.

DATE - Month/day/year on which the data was taken.

The following data cards contain the actual counts as well as the total number of laser firings used to produce those counts. Different gas types are input on separate data cards. If operation is under dual channel mode, blanks are left on each data card for those alternate bins which do not apply to that particular gas. Also included on these data cards are data, run number and gas type for easy identification purposes.

III. DATA REDUCTION

A. Pile-up Correction

Data cards are read in and count rates from each bin are corrected for system pile-up error:

$$F_{obs} = F_{real} \exp(-F_{real}/f)$$

where F_{obs} = observed count rate (i.e., counts/laser firings X time width)

F_{real} = actual count rate after pile-up correction

f = rate correction term (presently equals 126 MHz)

The pile-up correction subroutine (TRANS) uses the Newton-Raphson iterative method to solve the above equation within an absolute error of .001. After a solution is found, the actual rates are converted back to counts and transfer is made back to the main program. Corrected bin counts for each gas type are then accumulated into two arrays (CNT1 and CNT2).

B. Averaging and Range Correcting

The last card in the data deck is a blank card which signals the program that there is no more data. Data is then averaged if needed due to multiple runs. If in laser pulsed mode, range corrected:

$$R_i = BT + (\tau/2) + (i-1) \times \tau \qquad i = 1, 16$$

where R_i = range of each of 16 bins (usec)

BT = begin time

τ = time width

$$R^2\overline{CTN}_i = R_i^2 \left(\sum_{j=1}^{N} CNT_{ij} \Big/ \sum_{j=1}^{N} NOS_j\right) \qquad i = 1, 16$$

where CNT_{ij} = counts of a particular gas (i ranges through the bins and j ranges through the different runs)

NOS_j = total number of shots for j^{th} run

N = total number of runs

And the Poisson error for a particular gas type and bin is:

$$E_{g_i} = R_i^2 \sqrt{\sum_{j=1}^{n} CNT_{ji}} \Big/ \sum_{j=1}^{n} NOS_j$$

Program checks the standard lamp parameter ISTL, and if turned on sets R_i^2 to one to cancel the range correction factor in the above and following equations.

C. Exponential Fit

Exponentials are then fitted to the data using a least squares technique. Blank bins (either due to system overflow or to dual channel operation) are not included in the fit. If we define:

$$X_i = R_i^2$$

$$Y_i = \ln R^2 \overline{CNT}_i$$

$$W_i = \left(\sum_{j=1}^{m} E_{g_j}^2\right) / E_{g_i}^2 \qquad i=1,m \quad m \leq 16$$

then a library subprogram will fit a linear curve by minimizing the sum of the residuals:

$$\sum_{i=1}^{m} r_i^2 = \sum_{i=1}^{m} W_i [(a_o + a_1 X_i) - Y_i]^2.$$

Once the exponentials have been calculated, blank values are replaced by the fit values. Standard error for the exponential fits are determined by the sum of the residuals:

$$E_e = \sqrt{\sum_{i=1}^{m} r_i^2 \Big/ \left(\sum_{i=1}^{m} W_i\right) (m-1)}$$

D. Ratioing

Ratios of TYPE1 to TYPE2 gases and deviations on the ratios are calculated:

$$R12_i = \overline{CNT}_{1_i} / \overline{CNT}_{2_i}$$

$$E_{R12_i} = \sqrt{1/\overline{CNT}_{1_i} + 1/\overline{CNT}_{2_i}} \; R12_i \qquad i=1, 16$$

Finally, the weighted ratio mean and its standard error are given by:

$$W12_i = \left(\sum_{j=1}^{16} E^2_{R12_j}\right) / E^2_{R12_i} \qquad i=1, 16$$

$$\overline{R12} = \left(\sum_{j=1}^{16} W12_j \; R12_j\right) / \sum_{j=1}^{16} W12_j$$

$$E_{\overline{R12}} = \sqrt{\sum_{j=1}^{16} W12_j \; (R12_j - \overline{R12})^2 \Big/ \sum_{j=1}^{16} W12_j \; (m-1)}$$

IV. OUTPUT

Computer print-out includes data input, pile-up corrected data, range corrected and averaged data and ratio data. Plot output includes curves for both types of gases as well as their exponential fits. If two gases are to be analyzed a ratio plot is also drawn. Also printed out on the plots are the exponents and ratio with their estimates of error.

Carolyn F. Jones
LTV/HTC

bcs

DATA CARD SPECIFICATIONS

Card No. 1

Variable Name	Description	Columns
BT	Begin time (usec)	1 - 6
TAU	Time width (usec)	7 - 12
F	Pile-up correction (126 MHz)	13 - 18
TYPE1	First type gas (e.g., N2, O2, CO2, etc)	19 - 22
TYPE2	Second type gas (leave blank if none)	23 - 26
IDUAL	Code = 1 for single channel mode = 2 for dual channel mode	28
ISTL	Code = 0 or blank for laser pulsed mode = 1 for standard lamp mode	30
DATE	Date of data (month/day/year)	33 - 40

(Note: For variables TYPE1 and TYPE2, if less than 4 letters, must be right justified. For example, N2 would be in columns 21 and 22 if TYPE1.)

EXAMPLES

Single Channel Laser Pulsed Mode (IDUAL=1, ISTL=0)

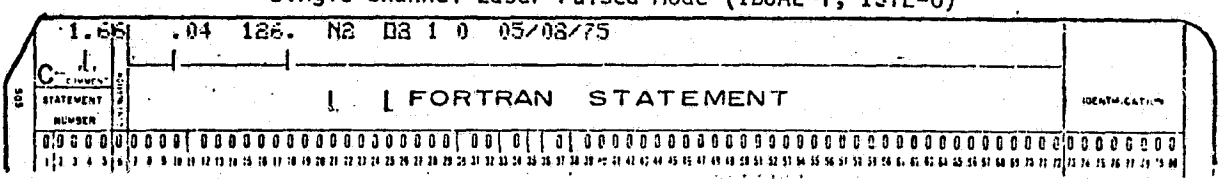

Dual Channel Laser Pulsed Mode (IDUAL=2, ISTL=0)

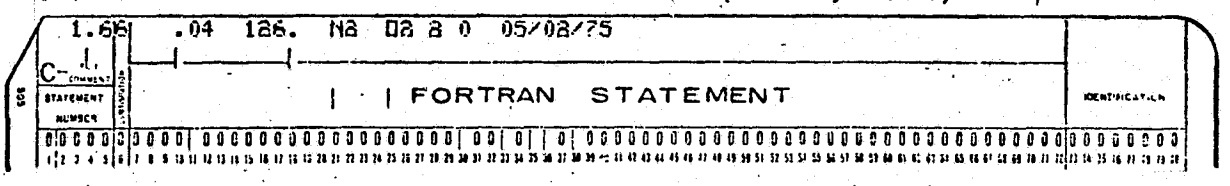

Single Channel Standard Lamp Mode (IDUAL=1, ISTL=1)

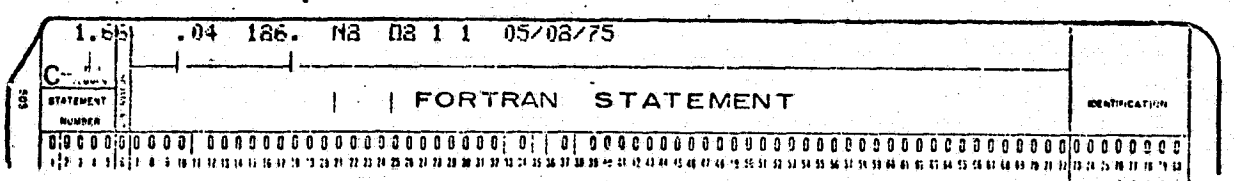

Dual Channel Standard Lamp Mode (IDUAL=2, ISTL=1)

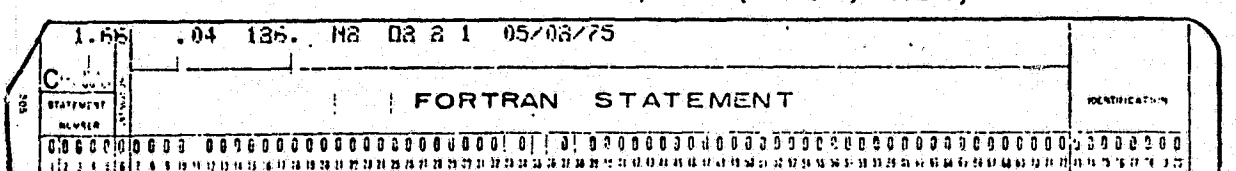

Cards No. 2

Variable Names	Description	Columns
DAYS	Date of data (month-day-year no slashes	1 - 6
RUN	Run number (right justified)	7 - 8
TYPE	Type gas (must match either TYPE1 or TYPE2, right justified)	9 - 12
NOS	Number of shots for that run (right justified)	13 - 16
DATA(i), i=1, 16	Counts from the 16 channels (each channel is alloted 4 columns on data card, right justified)	17 - 80

NOTE: Any number of this type data card is allowed. Program will average any number of runs of a particular gas. Different gas types must be on separate cards. Leave blank columns for overflow data and for alternate channels on dual channel data. Last data card must be followed by a blank card.

EXAMPLES

Single Channel - all bins filled

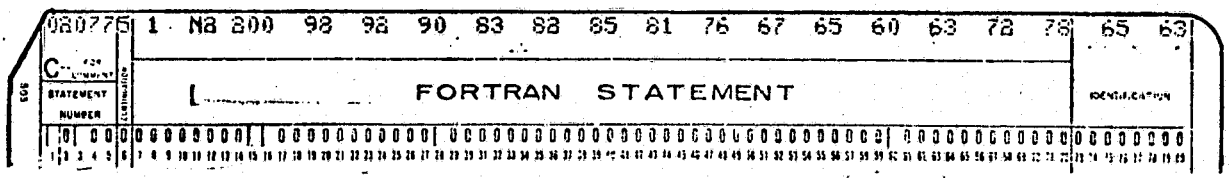

Dual Channel - alternate bins on each card left blank

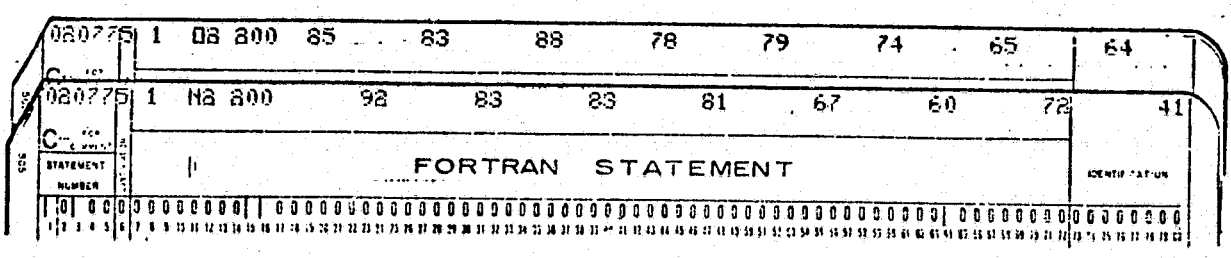

Single Channel - bin A left blank due to overflow

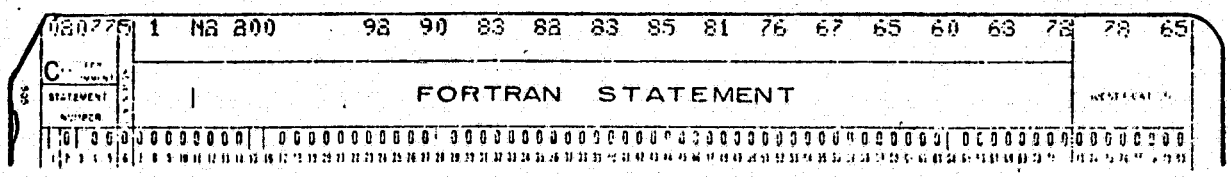

Sample data card set-up

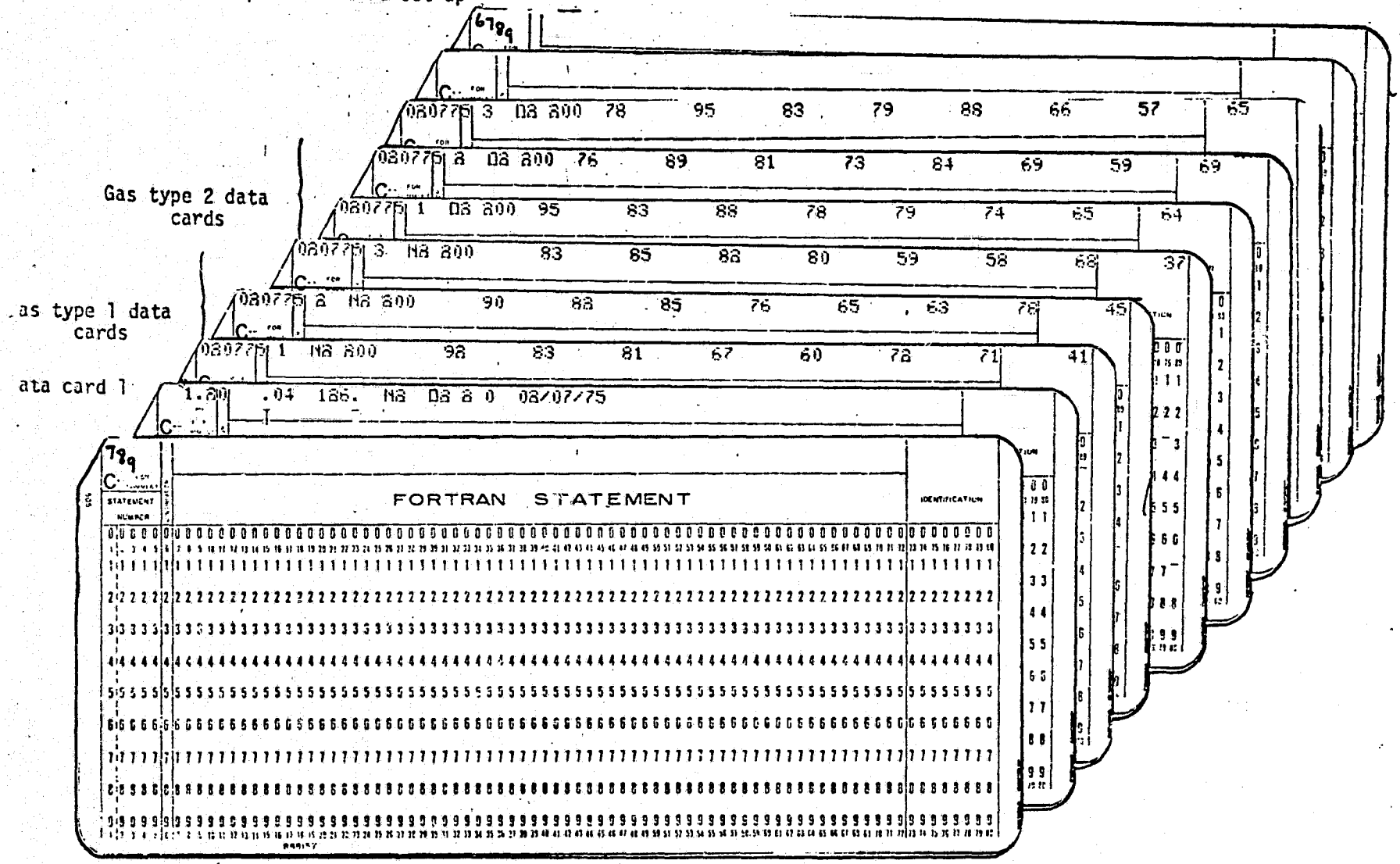

SAMPLE OUTPUT

DATE 05/02/75
MODE 1

(Note: Dual path range refers to the propagation to the backstop and return.)

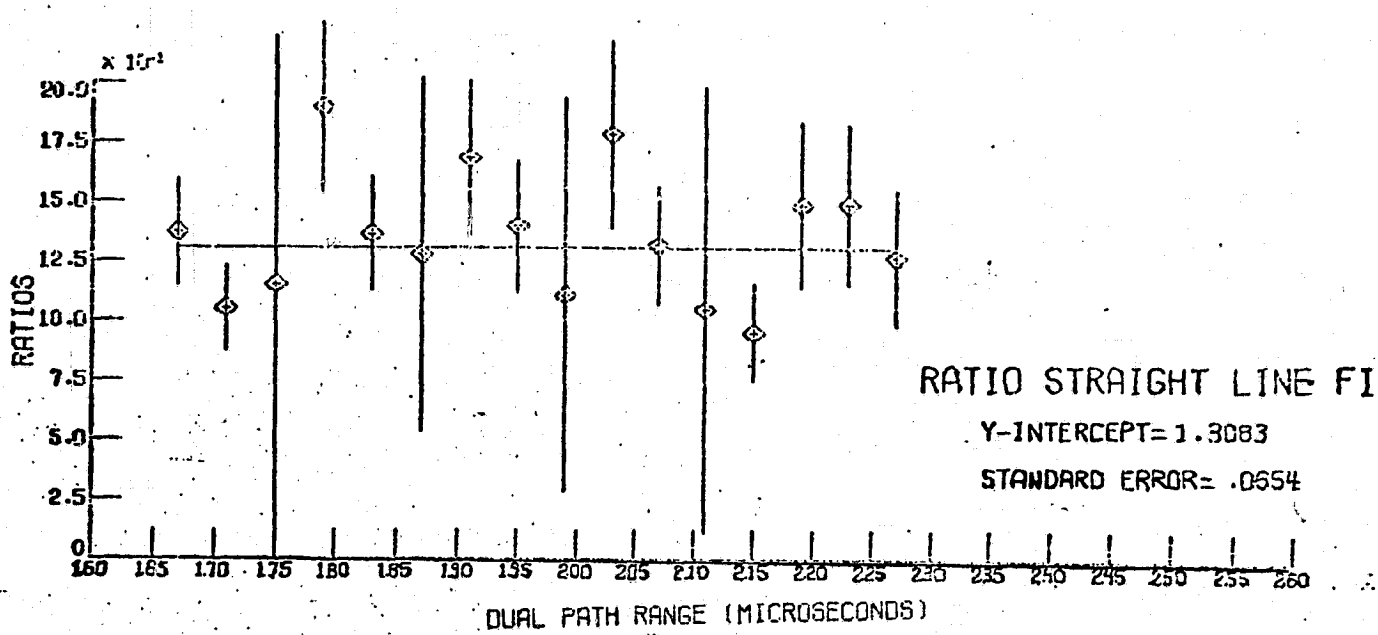

RATIO STRAIGHT LINE FI

Y-INTERCEPT= 1.3083

STANDARD ERROR= .0654

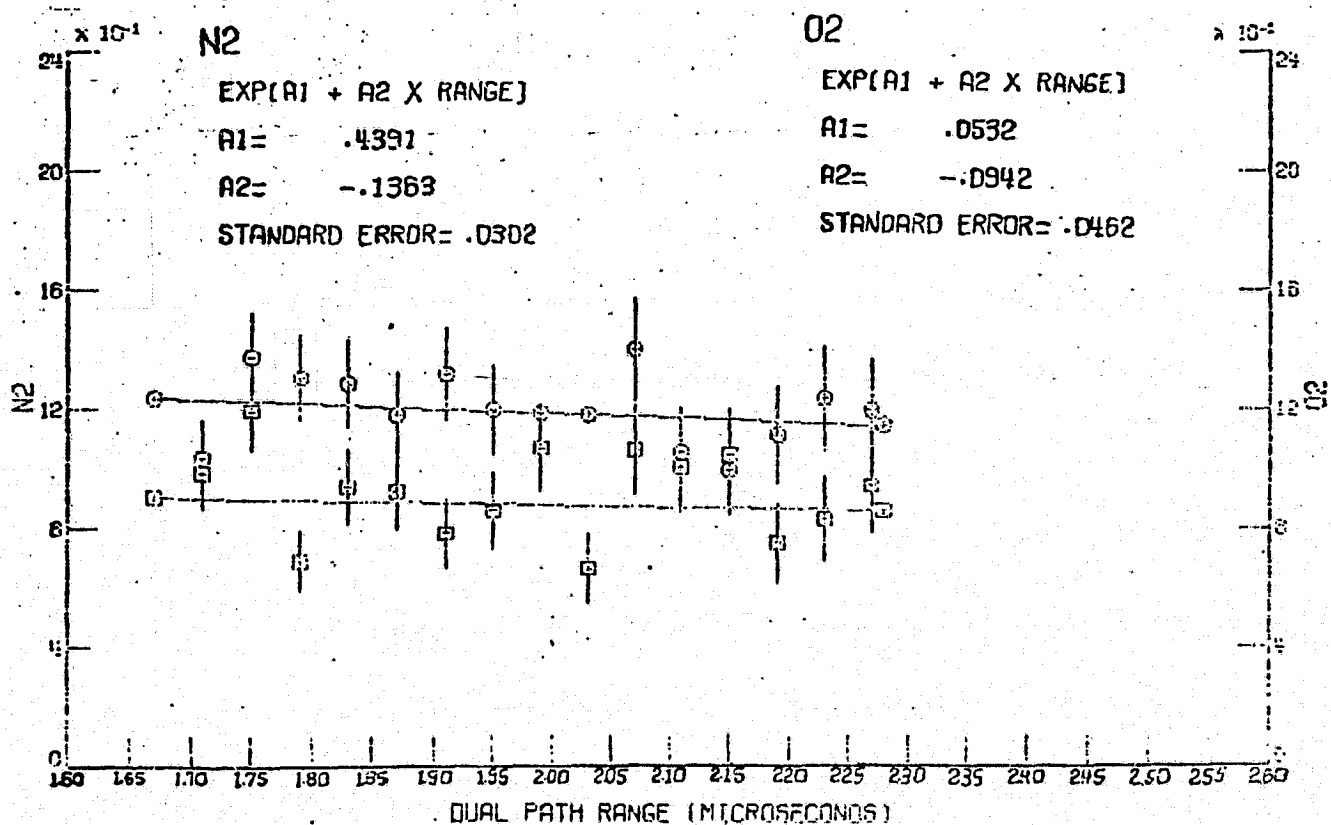

DATE 06/03/75
MODE 2

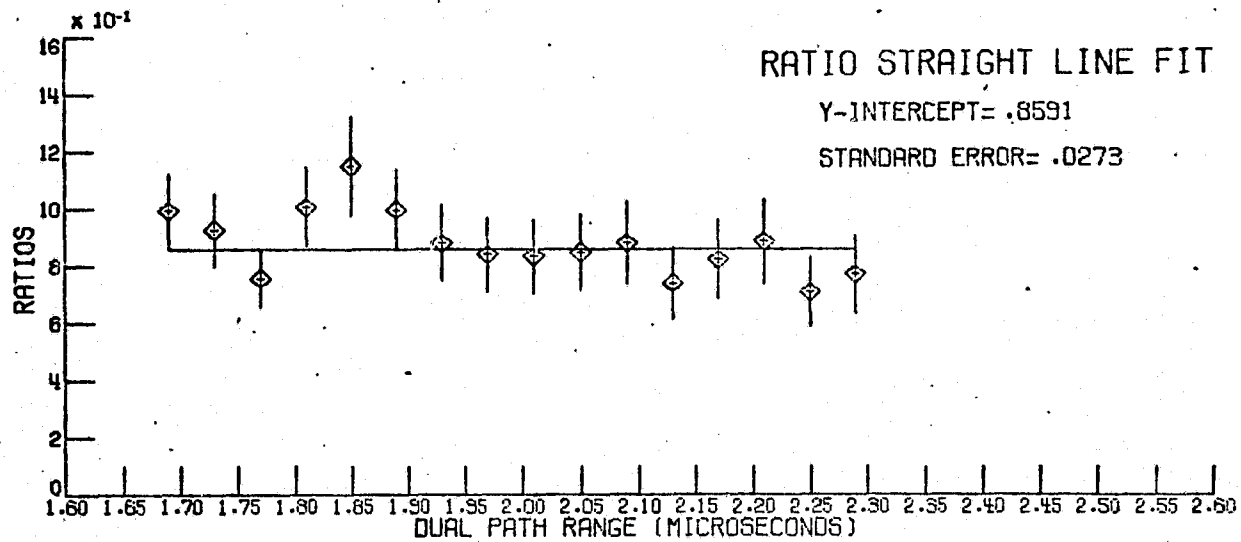

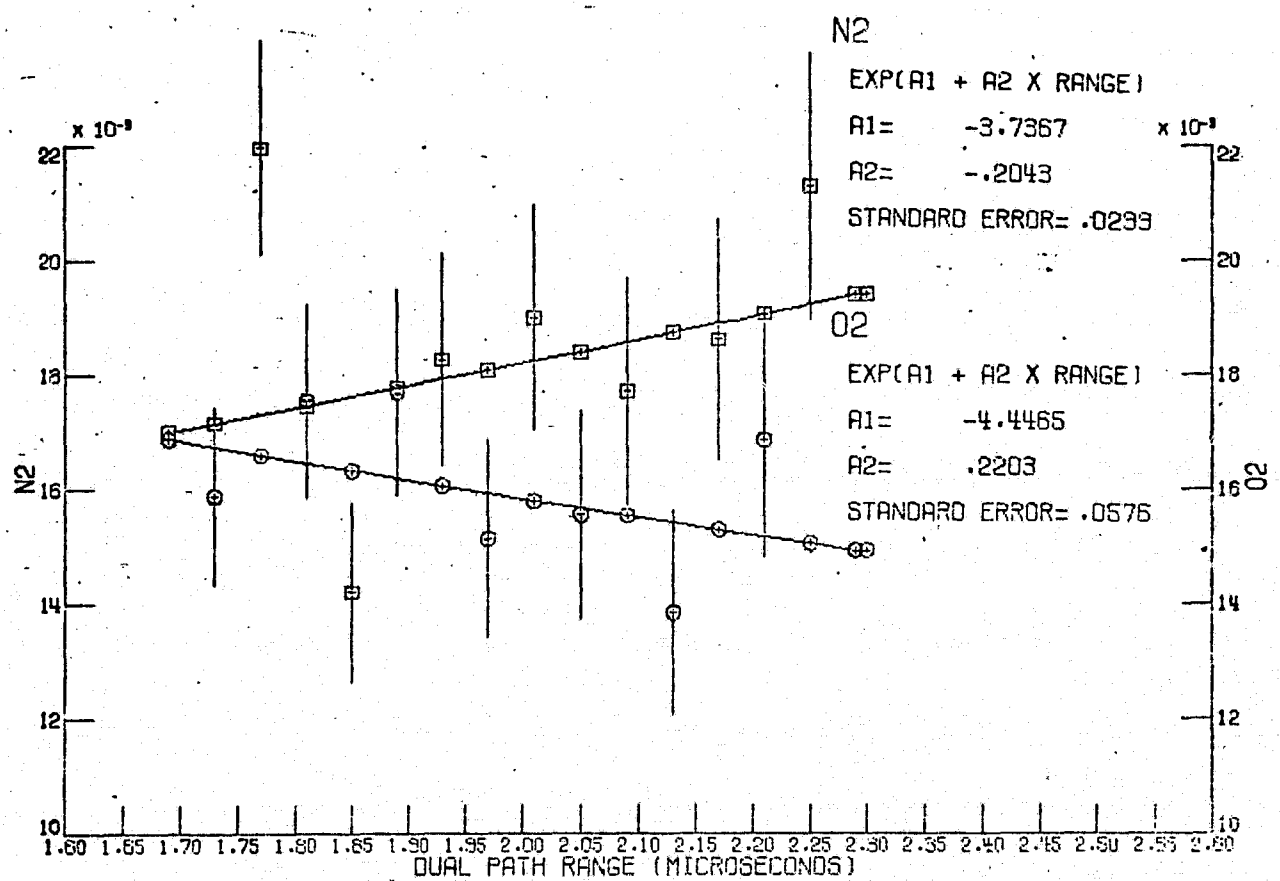

DATE 06/26/75
MODE 2
STD. LAMP CALIBRATION

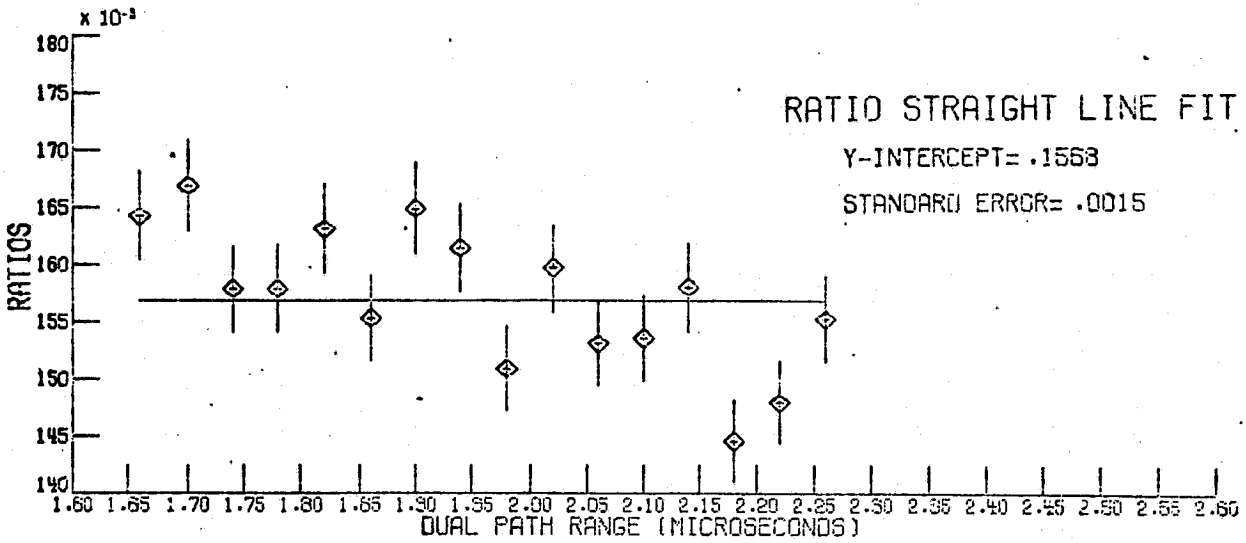

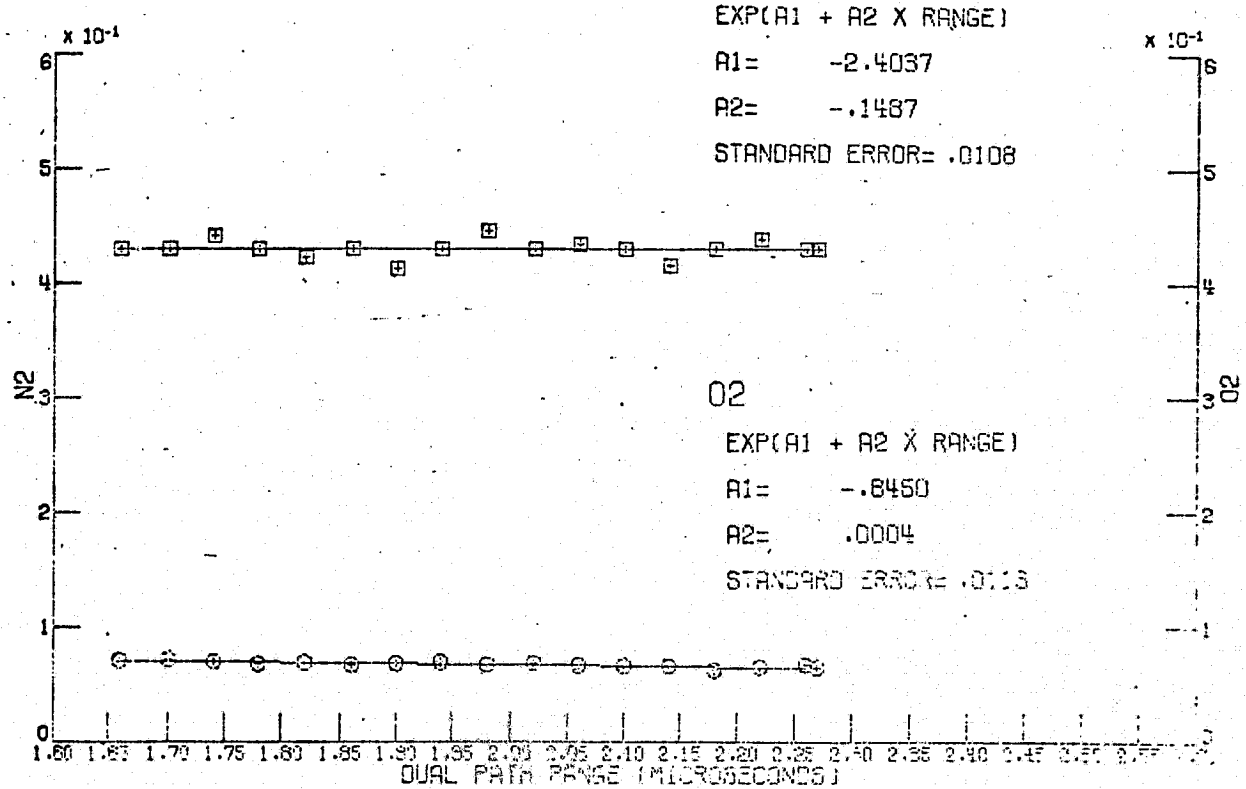

```
                      PROGRAM PCULT(INPUT,OUTPUT)
     CCCCC2           DIMENSION TIM(4),SIG(4)
     CCCCC3           DIMENSION Y(18,1),X(18),RESID(18,1),SUMSQ(1),A(2,2),B(2,1),C(2,1)
     CCCCC3           DIMENSION CNT1(18),CNT2(18),R(18),EG1(18),EG2(18),R12(18),DATA(34)
                     ,,ER12(18),WK(18,2),W(18),W12(18)
     CCCCC3           INTEGER RUN
                C  INITIALIZE VARIABLES TO ZERO
     CCCCC3           NOS1=NOS2=0
     CCCCC5           DO 1 I=1,16
     CCCCC7           CNT1(I)=CNT2(I)=R12(I)=EG1(I)=EG2(I)=ER12(I)=0.
     CCCCI7    1      CONTINUE
     CCCC20           READ 100, BT,TAU,F,TYPE1,TYPE2,IDUAL,ISTL,DATE
     CCCC44    100    FORMAT (3F6.2,2A4,2I2,2X,A8)
     CCCC44           PRINT 202, BT,TAU,F,TYPE1,TYPE2
     CCCC62    202    FORMAT (1H1,*DATA INPUT*/1X,*INITIAL DELAY=*,F5.3/1X,*RESOLUTION=*
                     ,,F6.3/1X,*F (PILE UP)=*,F9.3/1X,*GAS TYPES *,A10,*  AND*,A10)
     CCCC62           FTIME=BT+(TAU/2.)
     CCCC65    2      READ 101, DAYS,RUN,TYPE,NOS,(DATA(I),I=1,16)
     CCC1C7    101    FORMAT (A6,I2,A4,I4,16F4.0)
     CCC1C7           IF (RUN.EQ.0)GOTO 7
     CCC110           PRINT 203, DATE,RUN,TYPE,NOS,(DATA(I),I=1,16)
     CCC122    203    FORMAT (1X,*DATE*,A8,*  RUN*,I2,*  TYPE*,A6,*  NO.SHOTS*,I4,4X,16F
                     ,5.0)
     CCC132           IF (TYPE.EQ.TYPE1) 3,5
                C ACCUMULATE TYPE1 GAS
     CCC137    3      NOS1=NOS1+NOS
     CCC141           DO 4 I=1,16
     CCC142           IF (DATA(I).EQ.0.) GOTO 4
     CCC149           FCBS=DATA(I)
     CCC14E           CALL TRANS (FCBS,FREAL,F,TAU,NOS)
     CCC150           DATA(I)=FREAL
     CCC162           CNT1(I)=CNT1(I)+FREAL
     CCC166    4      CONTINUE
     CCC167           PRINT 212, (DATA(I),I=1,16)
     CCC171           GOTO 2
                C ACCUMULATE TYPE2 GAS
     CCC178    5      NOS2=NOS2+NOS
     CCC174           DO 6 I=1,16
     CCC175           IF (DATA(I).EQ.0.) GOTO 6
     CCC176           FCBS=DATA(I)
     CCC2C0           CALL TRANS (FCBS,FREAL,F,TAU,NOS)
     CCC2C3           DATA(I)=FREAL
```

```
CCC2C5          CNT2(I)=CNT2(I)+FREAL
CC0210    6     CONTINUE
CCC212          PRINT 212, (DATA(I),I=1,16)
CC0224          GOTO 2
          C RANGE CORRECT AND CALCULATE ERROR
CC0225    7     DO 11 I=1,16
CCC227          R(I)=ETIME+(I-1)*TAU
CCC234          TSQ=R(I)**2
CC0236          IF (ISTL.EQ.1) TSQ=1.
CCC241          IF (CNT1(I).EQ.C.) 9,8
CCC246    8     EG1(I)=SQRT(CNT1(I))/NCS1*TSQ
CC0254          ER12(I)=1./CNT1(I)
CCC256          CNT1(I)=CNT1(I)/NCS1*TSQ
CC0261    9     IF (CNT2(I).EQ.C.) 11,10
CCC266    10    EG2(I)=SQRT(CNT2(I))/NCS2*TSQ
CC0274          ER12(I)=1./CNT2(I)+ER12(I)
CCC277          CNT2(I)=CNT2(I)/NCS2*TSQ
CCC3C3    11    CONTINUE
CC0305          IF (ISTL.EQ.0) PRINT 206,TYPE1
CCC314          IF (ISTL.EQ.1) PRINT 207,TYPE1
CC0324          PRINT 205, (CNT1(I),I=1,16)
CCC326          PRINT 204, (EG1(I),I=1,16)
CC035C    2C4   FORMAT (1HC,55X,1CHDEVIATIONS/1X,16F8.2)
CC035C    2C5   FORMAT          (1H0,6X,*A*,7X,*B*,7X,*C*,7X,*D*,7X,*E*,7X,*F*,
               ,7X,*G*,7X,*H*,7X,*I*,7X,*J*,7X,*K*,7X,*L*,7X,*M*,7X,*N*,7X,*O*,7X,
               ,*P*/1X,16F8.2)
CCC35C    2C6   FORMAT (4(/)32X,*RANGE CORRECTED AVERAGES OF*,A6)
CC0350    2C7   FORMAT(4(/)32X,*STANDARD LAMP AVERAGES OF*,A6)
CCC35C          IF (ISTL.EQ.0) PRINT 206,TYPE2
CC0367          IF (ISTL.EQ.1) PRINT 207,TYPE2
CC0367          PRINT 205, (CNT2(I),I=1,16)
CCC4C1          PRINT 204, (EG2(I),I=1,16)
CC0413    212   FORMAT (20X,*AFTER PILEUP CORRECTION*,7X,16F5.1)
          C FIT EXPONENTIAL TO NITROGEN DATA
CC0413          WTSM=0.
CC0414          WSUM=0.
CC0415          DO 1201 I=1,16
CC0416    1201  WSUM=WSUM+EG1(I)**2
CCC422          L=0
CCC423          DO 1202 I=1,16
CCC425          IF (CNT1(I).EQ.C.) GOTO 1202
CCC426          L=L+1
CCC43C          W(L)=WSUM/EG1(I)**2
```

```
CC0433          Y(L)=ALOG(CNT1(I))
CC0436          X(L)=R(I)
CC044C          WTSM=W(L)+WTSM
CC0442   1202   CONTINUE
CC0444          LTOT=L
CC0446          CALL LSQPOL (18,LTOT,X,1,Y,W,2,2,RESID,SUMSQ,A,B,WK,IERR)
          C FILL IN ZEROES IN DATA WITH EXPONENTIAL FIT    (TYPE1)
CC0463          DO 120 I=1,16
CC0465          IF (CNT1(I).NE.C.) GOTO 120
CC0466          CNT1(I)=EXP(B(1)+B(2)*R(I))
CC0475          TSQ=R(I)**2
CC0477          IF (ISTL.EQ.1) TSQ=1.
CC05C2          ER12(I)=ER12(I)+TSQ/(CNT1(I)*NCS1)
CC05C7   120    P12(I)=CNT1(I)
CC0513          SUMSQ=SQRT(SUMSQ/(WTSM*(LTOT-1)))
CC0523          CALL PSEUDO
CC0524          CALL CALPLT (1.,1.,-3)
          C PRINT EXPONENTIAL DATA ON PLOT
CC0527          CALL NOTATE (12.,6.,.2,TYPE1,0.,4)
CC0533          CALL NOTATE (12.5,5.6,.15,20HEXP(A1 + A2 X RANGE),C.,20)
CC0537          CALL NOTATE (12.5,5.2,.15,5HA1=  ,0.,5)
CC0543          CALL NUMBER (13.5,5.2,.15,B(1),0.,4)
CC0547          CALL NOTATE (12.5,4.8,.15,5HA2=  ,0.,5)
CC0553          CALL NUMBER (13.5,4.8,.15,B(2),0.,4)
CC0557          CALL NOTATE (12.5,4.4,.15,15HSTANDARD ERROR=,C.,15)
CC0563          CALL NUMBER (14.5,4.4,.15,SUMSQ,0.,4)
CC0567          IF (NCS2.EQ.0) GOTO 322
          C FIT EXPONENTIAL TO OXYGEN DATA
CC057C          WTSM=SUMSQ=0.
CC0572          WSUM=0.
CC0573          DO 1206 I=1,16
CC0574          RESID(I)=0.
CC0575   1206   WSUM=WSUM+EG2(I)**2
CC06C1          L=0
CC06C2          DO 1207 I=1,16
CC06C4          IF (CNT2(I).EQ.C.) GOTO 1207
CC06C5          L=L+1
CC06C7          W(L)=WSUM/EG2(I)**2
CC0612          Y(L)=ALOG(CNT2(I))
CC0615          X(L)=R(I)
CC0617          WTSM=W(L)+WTSM
CC0621   1207   CONTINUE
CC0623          LTOT=L
```

```
      CALL LSQPCL (18,LTCT,X,1,Y,W,2,2,RESID,SUMSQ,A,C,WK,IERR)
C FILL IN ZEROES IN DATA WITH EXPONENTIAL FIT    (TYPE2)
      DO 122 I=1,16
      IF (CNT2(I).NE.0.) GOTO  121
      CNT2(I)=EXP(C(1)+C(2)*R(I))
      TSQ=R(I)**2
      IF (ISTL.EQ.1) TSQ=1.
      ER12(I)=ER12(I)+TSQ/(CNT2(I)*NCS2)
121   R12(I)=R12(I)/CNT2(I)
      ER12(I)=SQRT(ER12(I))*R12(I)
122   CONTINUE
      SUMSQ=SQRT(SUMSQ/(WTSM*(LTCT-1)))
      PRINT 208
208   FORMAT (4(/)32X,*RATIOS OF TYPE1 TO TYPE2 GAS*)
      PRINT 205,(R12(I),I=1,16)
      PRINT 204, (ER12(I),I=1,16)
C PRINT EXPONENTIAL DATA ON PLOT
      CALL NOTATE (12.,3.,.2,TYPE2,0.,4)
      CALL NOTATE (12.5,2.6,.15,20HEXP(A1 + A2 X RANGE),0.,20)
      CALL NOTATE (12.5,2.2,.15,5HA1=  ,0.,5)
      CALL NUMBER (13.5,2.2,.15,C(1),0.,4)
      CALL NOTATE (12.5,1.8,.15,5HA2=  ,C.,5)
      CALL NUMBER (13.5,1.8,.15,C(2),0.,4)
      CALL NOTATE (12.5,1.4,.15,15HSTANDARD ERROR=,0.,15)
      CALL NUMBER (14.5,1.4,.15,SUMSQ,0.,4)
322   CALL ASCALE (R,10.,16,1,10.)
      TIM(3)=XORG=R(17)
      TIM(4)=XS=R(18)
      CALL AXES(0.,0.,0.,10.,XORG,XS,.5,0.,8HCHANNELS,.15,-8)
C PUT ALL TYPE1 AND TYPE2 GASES IN ONE ARRAY AND CALCULATE ORIGIN AND SCALE
      J=0
      DO 1100 I=1,16
      DATA(J+1)=CNT1(I)
      IF (NCS2.EQ.0) CNT2(I)=CNT1(I)
      DATA(J+2)= CNT2(I)
      J=J+2
1100  CONTINUE
      CALL ASCALE (DATA,6.,32,1,10.)
      CNT1(17)=CNT2(17)=SIG(3)=YORG=DATA(33)
      CNT1(18)=CNT2(18)=SIG(4)=YSC=DATA(34)
      CALL AXES ( 0.,0.,90.,6.,YORG,YSC,1.,0.,TYPE1,.15,4)
      CALL AXES (10.,0.,90.,6.,YORG,YSC,1.,0.,TYPE2,.15,-4)
C PLOT GAS TYPE1
```

```
CC11C7   123    CALL LINPLT(R,CNT1,16,1,-1,11,1,0)
CC1117          DC 110 I=1,16
CC1121          TIM(1)=TIM(2)=R(I)
CC1124          SIG(1)=CNT1(I)-EG1(I)
CC1128          SIG(2)=CNT1(I)+EG1(I)
CC113C          CALL LINPLT (TIM,SIG,2,1,0,0,.1,0)
CC114C   110    CONTINUE
        C PLCT EXPONONTIAL FIT TC GAS TYPE1
CC1142          DC 1205 I=1,16
CC1144   1205   CNT1(I)=EXP(B(1)+B(2)*R(I))
CC1155          CALL LINPLT (R,CNT1,16,1,0,11,1,0)
CC1164          IF (NOS2.EC.0) GCTO 55
        C PLCT GAS TYPE2
CC1165          CALL LINPLT (R,CNT2,16,1,-1,12,1,0)
CC1175          DC 12 I=1,16
CC1177          TIM(1)=TIM(2)=R(I)
CC12C2          SIG(1)=CNT2(I)-EG2(I)
CC12C4          SIG(2)=CNT2(I)+EG2(I)
CC12C6   12     CALL LINPLT (TIM,SIG,2,1,0,0,.1,C)
        C PLCT EXPONONTIAL FIT TC GAS TYPE2
CC1220          DC 1210 I=1,16
CC1222   121C   CNT2(I)=EXP(C(1)+C(2)*R(I))
CC1233          CALL LINPLT (R,CNT2,16,1,0,12,1,0)
CC1242          CALL CALPLT (C.,8.,-3)
        C PLCT RATIC OF GAS TYPE1 TC GAS TYPE2
CC1245          CALL ASCALE (R12,4.,16,1,10.)
CC1251          CRG=SIG(3)=R12(17)
CC1254          SC=SIG(4)=R12(18)
CC1256          CALL AXES(0.,0.,0.,10.,XORG,XS,.5,0.,6HCHANNELS,.15,-6)
CC1271          CALL AXES (0.,0.,90.,4.,CRG,SC,.5,0.,6HRATICS,.15,6)
CC13C4          CALL LINPLT (R,R12,16,1,-1,13,1,0)
CC1314          DC 13 I=1,16
CC1316          TIM(1)=TIM(2)=R(I)
CC1321          SIG(1)=R12(I)-ER12(I)
CC1323          SIG(2)=R12(I)+ER12(I)
CC1325   13     CALL LINPLT (TIM,SIG,2,1,0,0,.1,0)
        C FIT HORIZONTAL LINE TC RATIC DATA
CC1337          SUM=WSUM=0.
CC1341          DC 1211 I=1,16
CC1343   1211   WSUM=WSUM+ER12(I)**2
CC1347          L=0
CC135C          DC 1212 I=1,16
CC1352          L=L+1
```

```
CC1354          W12(L)=WSUM/ER12(I)**2
CC1357          Y(L)=R12(I)
CC1360          X(L)=R(I)
CC1362   1212  CONTINUE
CC1363          LTCT=L
CC1364          WTSM=RESID=SUM=0.
CC1367          DO 1213 L=1,LTCT
CC1370          WTSM=WTSM+W12(L)
CC1372          SUM=SUM+Y(L)*W12(L)
CC1375   1213  CONTINUE
CC1377          YINTC=SUM/WTSM
CC1401          DO 1214 L=1,LTCT
CC1403          RESID=RESID+W12(L)*(Y(L)-YINTC)**2
CC1413   1214  CONTINUE
CC1416          STER=SQRT(RESID/(WTSM*(LTCT-1)))
CC1425          DO 1215 I=1,16
CC1426   1215  W12(I)=YINTC
                C PLOT STRAIGHT LINE FIT
CC1431          CALL LINPLT (R,R12,16,1,0,0,1,0)
CC1441          CALL NOTATE (12.,1.0,.2,23HRATIO STRAIGHT LINE FIT,0.,23)
CC1445          CALL NOTATE (12.5,  .6,.15,12HY-INTERCEPT=,0.,12)
CC1451          CALL NUMBER (14.1,  .6,.15,YINTC,0.,4)
CC1455          CALL NOTATE (12.5,  .2,.15,15HSTANDARD ERROR=,0.,15)
CC1461          CALL NUMBER (14.5,  .2,.15,STER,0.,4)
CC1465   99     IF (NOS2.EQ.0) CALL CALPLT (0.,8.,-3)
CC1471          CALL NOTATE (12.,3.5,.2,4HDATE,0.,4)
CC1475          CALL NOTATE (12.5,3.5,.2,DATE,0.,8)
CC1501          CALL NOTATE (12.,3.1,.2,4HMODE,0.,4)
CC1505          IDUAL=IDUAL
CC1507          CALL NUMBER (12.5,3.1,.2, IDUAL,0.,-1)
CC1513          IF (ISTL.EQ.1) CALL NOTATE (12.,2.7,.2,21HSTD. LAMP CALIBRATION,0.
               ,,21)
CC1521          CALL CALPLT (0.,0.,999)
CC1524          STOP
CC1526          END
```

```
                    SUBROUTINE TRANS (FOBS,FREAL,F,RESC,NCS)
0000 10             FOF(Z)=ZOBS-Z*EXP(Z/G)
0000 25             FOFP(Z)=EXP(Z/G)*(Z/F-1.)
0000 42             X1=ZOBS=FOBS/(RESC*NCS)
0000 46             G=-F
0000 47             DO 10 K=1,10
0000 50             KK=K
0000 51             X2=X1-FOF(X1)/FOFP(X1)
0000 61             IF (ABS(X2-X1).LT.10.E-3) GOTO 20
0000 65             X1=X2
0000 66    10       CONTINUE
0000 70    20       FREAL=X2
0000 71             FREAL=FREAL/ZOBS*FOBS
0000 73             RETURN
0000 74             END
```